Climate Dynamics

The impacts of oceanic deep temperature perturbations in the North Atlantic on decadal climate variability and predictability

--Manuscript Draft--

Manuscript Number:	CLDY-D-17-00085R2
Full Title:	The impacts of oceanic deep temperature perturbations in the North Atlantic on decadal climate variability and predictability
Article Type:	Original Article
Keywords:	Decadal climate predictability; initial condition uncertainties; linear optimal perturbation; North Atlantic variability; Atlantic meridional overturning circulation; IPSL-CM5A
Corresponding Author:	Agathe Germe, Dr. Meteo-France/CNRM Toulouse, FRANCE
Corresponding Author Secondary Information:	
Corresponding Author's Institution:	Meteo-France/CNRM
Corresponding Author's Secondary Institution:	
First Author:	Agathe Germe, Dr.
First Author Secondary Information:	
Order of Authors:	Agathe Germe, Dr.
	Florian Sévellec
	Juliette Mignot
	Alexey Fedorov
	Sébastien Nguyen
	Didier Swingedouw
Order of Authors Secondary Information:	

| Abstract: | Decadal climate predictability in the North Atlantic is largely related to ocean low frequency variability, whose sensitivity to initial conditions is not very well understood. Recently, three-dimensional oceanic temperature anomalies optimally perturbing the North Atlantic Mean Temperature (NAMT) have been computed via an optimization procedure using a linear adjoint to a realistic ocean general circulation model. The spatial pattern of the identified perturbations, localized in the North Atlantic, has the largest magnitude between 1000-4000m depth. In the present study, the impacts of these perturbations on NAMT, on the Atlantic meridional overturning circulation (AMOC), and on climate in general are investigated in a global coupled model that uses the same ocean model as was used to compute the three-dimensional optimal perturbations. In the coupled model, these perturbations induce AMOC and NAMT anomalies peaking after 5 and 10 years, respectively, generally consistent with the ocean-only linear predictions. To further understand the impact of these optimal perturbations, their magnitude was varied in a broad range. For initial perturbations with a magnitude comparable to the internal variability of the coupled model, the model |

response exhibits a strong signature in sea surface temperature (SST) and precipitation over North America and the Sahel region. The existence and impacts of these ocean perturbations have important implications for decadal prediction: they can be seen either as a source of predictability or uncertainty, depending on whether the current observing system can detect them or not. In fact, comparing the magnitude of the imposed perturbations with the uncertainty of available ocean observations such as Argo data or ocean state estimates suggests that the largest perturbations used in this study could be detectable. This highlights the importance for decadal climate prediction of accurate ocean density initialisation in the North Atlantic at intermediate and greater depths.

Response to reviewers' comments:

We thank both reviewers for their general positive comments. Please find in the following our actions in response to their suggestions, which further improved our manuscript. Our responses appear in blue color.

Reviewer #2:

The authors have satisfactory addressed all my previous comments. The manuscript is substantially improved after revision. Though, still there are some minor remarks (please see below). Additionally, I would suggest proofreading for Sections 2, 3 and figure captions.

We thank the reviewers for this comment and we have now carefully proofread sections 2 and 3 and the figure captions.

Lastly, I recommend this manuscript for acceptance and publication in Climate Dynamics after some minor revision.

Minor suggestions and comments:

L140: Add in the sentence "response ... to perturbation".
Done.

L186: Remove "during"
Done.

L187: Overall they are not generated the same way. To be more precise one could write "All ensembles use noise disturbance applied to SST field ...". And later in L193 you could then further specify "In addition to this atmospheric perturbation, six ensembles utilize full-depth oceanic temperature perturbations..."
Following these nice and precise suggestions we have modified the manuscript accordingly.

L317: "Western" -> western
Done.

L337: "european" -> European
Done.

L424: comma after LOP ?
Indeed, or else the grammatical structure of the sentence is not correct.

L443: comma after However
Done.

L445: comma after Therefore
Done.

L448: "ensemble generation perturbation strategies" -> ensemble generation (perturbation) strategies
Done.

L459 "consists on" -> is based on
Done.

L482: create an under- or overdispersive
Done.

L925-928: No need for all those details after "linear model". Suggest replacing with "as described by …"
Done.

L952 and L964: "with" -> with respect to
Done.

L955: "Precipitation" -> precipitation
Done.

L966: "surface atmospheric temperature" -> surface air temperature
Done.

Reviewer #3:

In my view, the authors have done very good job in addressing the constructive comments raised by the two previous reviewers.

What I am (still) puzzled with is that the perturbations have the largest magnitude below 1000m. I do not think that the authors make a convincing case, why this is dynamcially/physically reasonable; though I do understand that an explanation is beyond the scope here, but I think some brief speculations would be also good in the final part of the ms. I understand that other studies (e.g. Zanna et al) have found the same, and while I can follow their argument there, I am then wondering what we learn in addition here.

Our interpretation of this is that unlike surface anomalies, density anomalies induced in the deep ocean are able to persist over a sufficiently long time, maintaining meridional flow and amplifying the transient change of the AMOC (as discussed in Sévellec and Fedorov 2015). That explains the magnitude of the perturbations being greatest at depth. Zanna et al. is a very idealized study (flat bottom, rectangular basin, very idealized surface forcing), but they indeed found similar results possibly for the same physical reason. The fact that this mechanism holds in the fully coupled realistic climate model, albeit with a damping factor of the response of 3 is a new result.

We have added a brief discussion (l. 581-587) of this physical effect in the manuscript in the conclusion section.

Also, I feel that there is a mismacth between the ambitions/immediate relevance for initialized decadal predictions outlined at the end of the abstract and what is actually presented in the conclusions section. I would ask the authors to consider re-writing or extending this last part of the manuscript to make the overall context of this rather 'idealised' study clear.

We have added a short paragraph (l. 564-574) in the conclusion to insist that the potential teleconnections between the surface ocean and the atmosphere are still poorly represented in climate models, thereby limiting the applicability of the results for climate predictions. We have also added one sentence at the end of the paper to underline the fact that this study is idealized as compared to decadal predictions and that the exact link to decadal predictions is still to deepen.

1   **The impacts of oceanic deep temperature perturbations in the North Atlantic on decadal**

2   **climate variability and predictability**

3

4   Agathe Germe[1], Florian Sévellec[2], Juliette Mignot[3], Alexey Fedorov[4], Sébastien Nguyen[3],

5   Didier Swingedouw[5]

6

7   *[1] National Oceanography Centre, Southampton, SO14 3ZH, UK*

8

9   *[2] Ocean and Earth Science, University of Southampton, Southampton, UK*

10

11   *[3] LOCEAN Laboratory-IPSL, Sorbonne Universités (UPMC, Univ Paris 06)-CNRS-IRD-*

12   *MNHN, 4 place Jussieu, F-75005 Paris, France*

13

14   *[4] Department of Geology and Geophysics, Yale University, New Haven, CT, USA*

15

16   *[5] Environnements et Paléoenvironnements Océaniques et Continentaux (EPOC), UMR CNRS*

17   *5805 EPOC - OASU - Université de Bordeaux, Allée Geoffroy Saint-Hilaire, 33615 Pessac,*

18   *France*

19

20   Corresponding Author:
21   Agathe Germe
22   *National Oceanography Centre, Southampton*
23   *University of Southampton, Water Front Campus,*
24   *European Way*
25   *Southampton, SO14 3ZH*
26   *UK*
27   *agathe.germe@noc.ac.uk*

28

29

30

Abstract

Decadal climate predictability in the North Atlantic is largely related to ocean low frequency variability, whose sensitivity to initial conditions is not very well understood. Recently, three-dimensional oceanic temperature anomalies optimally perturbing the North Atlantic Mean Temperature (NAMT) have been computed via an optimization procedure using a linear adjoint to a realistic ocean general circulation model. The spatial pattern of the identified perturbations, localized in the North Atlantic, has the largest magnitude between 1000-4000m depth. In the present study, the impacts of these perturbations on NAMT, on the Atlantic meridional overturning circulation (AMOC), and on climate in general are investigated in a global coupled model that uses the same ocean model as was used to compute the three-dimensional optimal perturbations. In the coupled model, these perturbations induce AMOC and NAMT anomalies peaking after 5 and 10 years, respectively, generally consistent with the ocean-only linear predictions. To further understand the impact of these optimal perturbations, their magnitude was varied in a broad range. For initial perturbations with a magnitude comparable to the internal variability of the coupled model, the model response exhibits a strong signature in sea surface temperature (SST) and precipitation over North America and the Sahel region. The existence and impacts of these ocean perturbations have important implications for decadal prediction: they can be seen either as a source of predictability or uncertainty, depending on whether the current observing system can detect them or not. In fact, comparing the magnitude of the imposed perturbations with the uncertainty of available ocean observations such as Argo data or ocean state estimates suggests that the largest perturbations used in this study could be detectable. This highlights the importance for decadal climate prediction of accurate ocean density initialisation in the North Atlantic at intermediate and greater depths.

1. Introduction

The North Atlantic is one of the regions where near-term climate predictions are most promising (Kirtman et al., 2013). Such near-term climate predictions, on interannual to

65   decadal timescales, have a strong potential to influence our society with benefits to agriculture

66   (Hammer et al., 2001), energy supply strategies, adaptation to global climatic changes, *etc*.

67   However, these applications depend on the accuracy and reliability of the predictions (Slingo

68   and Palmer, 2011). In turn, the latter depends on a careful assessment of prediction

69   uncertainty. Indeed, in a perfect and therefore reliable prediction system, prediction

70   uncertainties and forecast errors are expected to be equal on average (Palmer et al., 2006). For

71   lead times shorter than a few decades, internal variability and model imperfections have been

72   shown to be the major contributors to the climate projection uncertainty in contrast to the

73   uncertainty arising from emission scenarios for greenhouse gases (Hawkins and Sutton,

74   2009). Near-term climate prediction experiments strive to reduce the projections uncertainty

75   by carefully initialising the climate system (Meehl et al., 2013). However, even for small

76   errors in the initial state, a large uncertainty may arise from the non-linearity of the system

77   (Lorenz, 1963). This source of uncertainty is usually taken into account by performing

78   ensemble predictions with slightly perturbed initial conditions.

79   Several ensemble generation techniques based on atmospheric perturbations only,

80   extending from random perturbations (e.g. Griffies and Bryan 1997; Persechino et al., 2013)

81   and shifting atmospheric state by a few days (e.g. Collins and Sinha, 2003; Collins et al.,

82   2006; Yeager et al., 2012), to more elaborated methods designed to generate optimal initial

83   perturbations, such as atmospheric singular vectors (e.g. Hazeleger et al., 2013) and breeding

84   vectors (e.g. Ham et al., 2014), have been used for decadal predictions and predictability

85   analyses. Although, all of these methods generate ensemble spread in the whole climate

86   system, they neglect uncertainties in the ocean initial state that need to be taken into account

87   at seasonal and decadal timescales. This may result in insufficiently dispersive ensembles

88   leading to overconfident and therefore unreliable forecasts (e.g. Ho et al., 2013). Despite these

89   generally accepted ideas, the inclusion of ocean state uncertainties in the initial ensemble

90   spread remains challenging.

91   Germe et al. (2017) compared the impact of atmospheric perturbations *versus* oceanic

92   perturbations and found that oceanic perturbations mimicking random oceanic uncertainties

93   have the same impact on the future evolution of the ensemble as atmospheric-only

94   perturbations after the first three months in the IPSL-CM5A-LR climate model. However, Du

95   et al. (2012) showed that oceanic perturbations arising from different assimilation runs do

96   affect the ensemble spread of oceanic-related variables. This latter result can be accounted for

97   by the differences between initial oceanic states of individual ensemble members that have

98   pronounced three-dimensional (3D) structure, contrasting the homogeneous white noise
99   perturbations applied by Germe et al. (2017).

100   Ocean initial condition uncertainties and their impacts on climate prediction have been
101   also addressed through bred vectors (Baehr and Piontek, 2014) and anomaly transform
102   methods (Romanova and Hense, 2016) yielding a weak improvement of prediction reliability
103   at seasonal timescales. Recently, Marini et al. (2016) have achieved a greater ensemble spread
104   for sea surface temperature (SST) during the first 3 years of simulations when oceanic
105   singular vectors are used rather than atmospheric-only perturbations. However, for more
106   integrated measures, such as the North Atlantic SST or the Atlantic Meridional Overturning
107   Circulation (AMOC), the ensemble spread is overestimated initially but decreases over time.

108   Several studies highlight the strong impact of the 3D structure of ocean state initial
109   errors and emphasize the sensitivity of North Atlantic decadal variability to initial conditions
110   in the deep ocean (Zanna et al. 2011; Palmer and Zanna 2013; Sévellec and Fedorov 2013a;
111   2013b; 2017). These analyses, based on the singular vectors decomposition (SVD, e.g. Zanna
112   et al. 2011; Palmer and Zanna 2013) or the linear optimal perturbations framework (LOP;
113   Sévellec et al. 2007; Sévellec and Fedorov 2013b; 2017), compute small initial perturbations
114   that induce the maximum response in the system after a specific time. While the SVD method
115   requires solving an eigenvalue problem, the LOP method relies on an optimization problem
116   producing the maximum linear growth of a chosen climatic variable. By construction, both
117   SVD and LOP methods, as applied to the ocean, are based on a linearization of the primitive
118   equations of motion and neglect potential effects of the ocean-atmosphere coupling together
119   with stochastic noise arising from atmospheric synoptic variability. Therefore, assessing the
120   impact of these structures within the full ocean-atmosphere climate system is necessary to
121   better understand their potential for climate prediction.

122   In this study, we investigate for the first time the impact of LOPs on climate
123   variability in a fully coupled Earth system model IPSL-CM5A-LR (Dufresne et al. 2013). We
124   apply the LOP framework maximizing changes in the North-Atlantic mean temperature
125   (NAMT) as described in Sévellec and Fedorov (2017). In the ocean model they used, the most
126   efficient LOP induces a NAMT anomaly that reaches its maximum after 10 years. The
127   optimization problem made use of the tangent linear forward and adjoint versions of the ocean
128   component of IPSL-CM5A-LR.

129   The LOPs dynamics are ultimately related to the excitation of an ocean basin mode
130   identified in the same linear model by Sévellec and Fedorov (2013b). This oscillatory mode
131   involves the westward propagation of subsurface density anomalies across the North Atlantic

132   basin. This propagation impacts the AMOC *via* thermal wind balance and basin-scale

133   variations of the zonal density gradient. There is evidence of a similar westward propagation

134   in the North Atlantic observations of sea-level height (e.g. Tulloch et al. 2009; Vianna and

135   Menezes 2013), subsurface temperature (Frankcombe et al. 2008), and SST (Feng and

136   Dijkstra 2014) with a comparable basin-crossing time (~10 years) as estimated by Sévellec

137   and Fedorov (2013b). It has been also identified in nearly 20 models of the CMIP5 database

138   (Muir and Fedorov 2016). In IPSL-CM5A-LR in particular, this oceanic mode exhibits

139   interaction with convective activity, sea ice, and atmospheric circulation (Ortega et al., 2015).

140   In the present analysis, climate response to the LOP is investigated in terms of changes

141   in NAMT, the AMOC strength, SST, and atmospheric temperature and precipitation. We use

142   ensemble experiments in order to extract the signal of the LOP response from the atmospheric

143   stochastic noise in a perfect model configuration, therefore avoiding pollution of the signal by

144   model drift, and model imperfections. The ensemble experiments, the coupled system and the

145   LOP are described in more detail in section 2. The response of the system to the oceanic

146   perturbations is then described in section 3, while implications for near-term climate

147   prediction are discussed in section 4. Finally concluding remarks are given in the last section.

148

149

150   **2. Method**

151

152   2.1 Model

153

154   We use the IPSL-CM5A-LR climate model (Dufresne et al., 2013). It includes the

155   atmospheric general circulation model LMD5A (Hourdin et al., 2013) with a $1.875° \times 3.75°$

156   horizontal resolution and 39 vertical levels. It is coupled with the oceanic model NEMOv3.2

157   (Madec 2008) in the ORCA2 configuration corresponding to a nominal resolution of 2°,

158   enhanced over the Arctic and subpolar North Atlantic as well as around the Equator. There

159   are 31 vertical levels for the ocean with the highest resolution in the upper 150 m. It also

160   includes the sea ice model LIM2 (Fichefet and Maqueda 1997) and the biogeochemistry

161   model PISCES (Aumont and Bopp 2006). The coupling between the oceanic and atmospheric

162   components is achieved via OASIS3 (Valcke 2006). The reader is referred to the special issue

163   of Climate Dynamics (vol 40, issue 9–10) for a full discussion of various aspects of this

164   climate model. The characteristics of the oceanic component of the coupled model are also

165   discussed in Mignot et al. (2013).

166　　　　This model has been used for several decadal prediction studies. In a perfect model

167　　context, it exhibits an average predictability limit for the annual AMOC of about 8 years with

168　　variations depending on the AMOC initial state (Persechino et al. 2013). The longest potential

169　　predictability of SST reaches up to 2 decades and is found in the North Atlantic Ocean, which

170　　is related to decadal AMOC fluctuations. These fluctuations are successfully initialized by

171　　nudging the SST field to observations (Swingedouw et al. 2013; Ray et al. 2014). This

172　　initialization could be further improved, in a perfect model framework, by additionally

173　　nudging sea surface salinity (SSS) (Servonnat et al. 2014) and taking into account the mixed

174　　layer depth when specifying the amplitude of the restoring coefficients (Ortega et al. 2017).

175　　Hindcasts starting from the SST nudged simulations exhibit a prediction skill up to one

176　　decade in the extratropical North Atlantic for SST and in the tropical and subtropical North

177　　Pacific for the upper-ocean heat content (Mignot et al., 2016).

178

179　　2.2 General approach

180　　　　　Firstly, we select a 20-year interval (model years 1991 to 2010) within the 1000-year

181　　long pre-industrial control simulation (thereafter CTL) of the IPSL-CM5A-LR model. This

182　　specific period is chosen because it does not exhibit strong variability either for the AMOC or

183　　NAMT, which both remain within one standard deviation from their 1000-year means. This is

184　　necessary to avoid internal variations that may complicate analysing the response to the

185　　applied perturbations. Seven ensembles of simulations are conducted using one single starting

186　　date – the 1st of January of this time period (model year 1991). All the ensembles are

187　　integrated forward for 20 years with a constant pre-industrial external forcing. All ensembles

188　　have a random noise disturbance applied to the SST field of the coupler, so that the SST of

189　　the ocean model is not directly perturbed as described in Persechino et al. (2013). The applied

190　　noise is identical for all ensembles. As this perturbed SST field is only used when SST is

191　　passed to the atmosphere during the integration first time step, this perturbation is considered

192　　as an atmospheric-only perturbation. Germe et al. (2017) showed that this method is

193　　equivalent to applying a random white noise to the whole oceanic temperature field. In

194　　addition to this atmospheric perturbation, six ensembles utilize full-depth oceanic temperature

195　　perturbations. The pattern of these perturbations corresponds to the LOP as computed by

196　　Sévellec and Fedorov (2017) using the tangent linear forward and adjoint versions of the same

197　　ocean model as in the coupled run. The six ensembles differ only by the magnitude and/or

198   sign of the oceanic perturbation pattern as described below (see Table 1 for details). The

199   seventh ensemble, without any perturbation to the oceanic temperature field, is taken as a

200   benchmark to assess the impact of oceanic perturbations in the other ensembles and will be

201   further referred to as ATM.

202   Throughout this analysis, the AMOC strength is defined as the maximum value of the

203   annual, zonal-mean stream function within 0-60°N and 500-2000m, while NAMT is defined

204   as a full depth average of the annual oceanic temperature over the North Atlantic within

205   30°N-70°N. The mean state and variability of CTL is assessed from the interannual average

206   and standard deviation for the entire 1000-year time series.

207   2.3 Oceanic perturbation pattern

208   The specific pattern of the 3D global oceanic temperature field used to perturb the

209   oceanic initial state of each ensemble has been computed by Sévellec and Fedorov (2017) as

210   optimally perturbing NAMT through the LOP methodology. They have used the adjoint of the

211   tangent linear version of the oceanic component of IPSL-CM5A-LR. More precisely, an

212   earlier version of the ocean component: OPA8.2 for which the adjoint version was available

213   at the time of the LOP computation. This LOP has been rationalized as the efficient

214   stimulation of the least damped oscillatory eigenmode of the tangent linear version of NEMO,

215   fully described in Sévellec and Fedorov (2013a). In particular, its location at depth, away

216   from strong velocities and density gradients (limiting mean- and self-advection, respectively),

217   allows for longer persistence of the anomaly and more efficient stimulation of the eigenmode.

218   This eigenmode corresponds to a 24-year oscillatory mode of both the AMOC and the NAMT

219   related to the westward propagation of large-scale temperature anomalies in the North

220   Atlantic. The basin-scale propagation influences the AMOC through its impact on the zonal

221   density gradient. Ortega et al. (2015) showed that in the IPSL-CM5A-LR coupled model, the

222   mode is maintained by a coupling with a surface mode of variability and potentially excited

223   by the atmosphere. Such coupling allows the intensification of the damped internal mode

224   through the excitation of the deep convection areas (Sévellec and Fedorov 2015).

225   By stimulating this variability mode, the LOP is the most efficient way to generate an

226   anomaly of the NAMT. The LOP pattern depends on the chosen time scale. In this study, we

227   use the LOP maximizing the NAMT response after 14 years in the linear model. In

228   accordance with the lag identified in Sévellec and Fedorov (2013a), corresponding to the time

229   needed for the AMOC to influence the NAMT, we expect an associated maximum response

230   of the AMOC after 8 years only. The LOP pattern exhibits the largest magnitudes in the North

231   Atlantic region (Figure 1), especially in the deep ocean (top *versus* bottom panels in Fig. 1).

232   These strongest magnitudes of the LOP are furthermore roughly co-located with areas of

233   strongest temperature variability in the North Atlantic in CTL (black lines in figure 1). In

234   Sévellec and Fedorov (2017), both temperature and salinity perturbation patterns are

235   identified. They have a constructive effect on the density anomaly field. In this study, we have

236   used only the temperature perturbation as a primary step to understand the response of the

237   coupled system to the LOP. The magnitude of the LOP shown in figure 1 corresponds, in the

238   linear model, to a NAMT response of approximately 43.8×10^{-3} °C after 14 years, which

239   corresponds to roughly one standard deviation of the NAMT in CTL (not shown). As the LOP

240   magnitude is determined by the linear model analysis, it is used as a reference to which

241   scaling factors of 1, 5, 10, 20, -10 and -20 are applied. At the initial date, these LOP

242   magnitudes sample the whole range of CTL variability regarding NAMT index. The naming

243   of the ensemble reflects this protocol. For example, P20 corresponds to the ensemble using

244   the positive version of the LOP as shown in figure 1, but with its magnitude multiplied by 20,

245   while N20 uses a scaling factor of -20. P01 is therefore the ensemble using the LOP exactly as

246   described in figure 1, and would lead to one standard deviation response of the NAMT after

247   14 years in the linear ocean-only model.

248

249   **3 Impact on the climate variability**

250

251   3.1 Response in the ocean

252

253   The climate model ensembles show that the LOP induces a NAMT anomaly reaching

254   its maximum value roughly ten years later (Figure 2, *top left panels*). In accordance with the

255   adjoint model analysis, it is preceded by a maximum anomaly of the AMOC 5 years earlier

256   (Figure 2, *bottom left and middle panels*). The link between these two responses will be

257   detailed below. For both the NAMT and AMOC, the magnitude of the response increases

258   linearly with the magnitude of the perturbation (Figure 2, *right panels*). The response is

259   significantly different from the ATM ensemble - according to a t-test at the 99% confidence

260   level - only for the largest perturbations, i.e. N20 and P20 (Figure 2, *middle and right panels*).

261   However, the linearity of the response suggests that significant response could be identified

262   for weaker magnitudes by increasing the ensemble size and therefore the robustness of the

263   statistical test. The AMOC response to the LOP looks slightly asymmetric, being weaker for

264   negative (N10 and N20) than positive (P10 and p20) LOP. However, when taking into

265   account the confidence interval of the ensemble means, this asymmetry is not significant at

266   the 95% level (Figure 2: *bottom right panel*). Such linearity through the whole range of

267   perturbation magnitudes might be noteworthy in a fully ocean-atmosphere coupled system,

268   which includes a large amount of non-linear processes.

269   Although linear, the response is also damped by roughly a factor 3 as compared to the

270   response of the linear ocean-only model (Figure 2, *gray shading* on the *top right panel*) and

271   occurs slightly earlier than expected (delay of 10 years instead of 14 years for the NAMT).

272   Quantitative differences in the response to the LOP in the fully coupled model as compared to

273   the ocean-forced context are indeed expected, although difficult to foresee. Atmospheric

274   stochastic noise is absent in the oceanic-forced context. In the fully coupled model used here

275   the perturbation pattern in the surface layer is on the contrary rapidly distorted by air-sea

276   interactions (Germe et al., 2017), which tends to limit the influence of the LOP pattern to its

277   deeper layers. Also, ensemble members differ from each other by their atmospheric states,

278   which leads to significant differences in air-sea interactions and in the upper ocean. Hence the

279   ensemble average tends to smooth-out the signature of the LOP in the upper ocean.

280   Consistently, the North Atlantic mean temperature of the first 300 m (NAMT300) is very

281   close to the one in ATM during the first 2 and 4 years for P20 and N20 respectively (Figure 3,

282   *top left panel*). Whereas, over the full oceanic depth, NAMT diverges as early as the first year

283   (Fig 2, top left panel).

284   Despite this weak initial perturbation in the upper layer, the response of NAMT300 to

285   the LOP is as significant as for the total NAMT (i.e. integrated over the whole water column)

286   after 10 years (figure 3, *top left panel*). Its spatial distribution exhibits a tripole/horseshoe

287   shape (figure 3, *middle and right panels*) that resembles the fingerprint of the AMOC with 5-

288   year lag in the model (figure 3, *bottom left panel*). This fingerprint pattern is consistent with

289   what can be inferred from SST observations (Dima and Lohman 2010). This suggests that this

290   upper layer response is mainly driven by the AMOC maximum response to the LOP at 5 years

291   forecast range. The influence of the LOP on the AMOC has been described by Sévellec and

292   Fedorov (2013b and 2015) in the tangent linear model and the involved mode of variability

293   has been identified by Ortega et al. (2015) in the control simulation using the same climate

294   model (i.e. CTL in this paper). In the present experiments, the LOP imposed in the North

295   Atlantic modulates the meridional density gradient, thereby favouring an acceleration of the

296   AMOC *via* thermal wind balance. The interaction of the resulting upper-ocean northward

297   flow and the mean meridional temperature gradient gives rise to a temperature anomaly in the

298   upper North Atlantic Ocean. It is the first time that this effect is prognostically tested and

299   highlighted in a fully comprehensive climate model. It confirms the strong sensitivity of the

300   upper ocean to temperature disturbances in the deep ocean, as described in Sévellec and

301   Fedorov (2013a; 2013b and 2017), in a coupled model. Such impact on the upper ocean

302   suggests some repercussions of the LOP onto the atmosphere in the North-Atlantic region.

303

304

305   3.2 Impact on the atmosphere

306

307   The impacts of the LOP on the annual mean SST exhibit a tripole pattern (Figure 4, 1st

308   *row*) similar to the response of the vertically integrated temperature over the first 300m

309   (T300; Figure 3, *top left panel*). The response to the positive LOP ensemble P20 is stronger

310   and larger scale than its negative equivalent ensemble N20. This is in accordance with the

311   AMOC response identified in the previous section and is associated with stronger atmospheric

312   impacts as well (*see other panels*). A significant impact is found on the 2-meter air

313   temperature (T2M), over the ocean, but also over land in some areas (Figure 4, 2nd *row*).

314   Apart from the eastern part of North America, the continental response to the positive and

315   negative LOP is not symmetric. For example, there is a significant response of T2M over the

316   Scandinavia for the P20 ensemble, which is not found significant for N20. A significant

317   impact is found over the western North Africa in N20, while it is found in the eastern North

318   Africa and Middle East regions in P20. These impacts on T2M persist throughout the year but

319   they are stronger in winter than in summer (Figure 5). For P20, T2M pattern evolves slightly

320   with the forecasting year, but the warm anomaly in the North-Atlantic region persists

321   throughout the first 15 years of the forecasting period.

322   In accordance with previous finding based on CTL (Persechino et al., 2013), AMOC

323   associated SST anomalies have a significant impact on summer precipitations over the Sahel

324   region (Figure 4, 3rd *row*). The positive LOP consistently induces an increase of summer

325   precipitation over the western African Sahel while the negative LOP impacts central and

326   eastern Sahelian region. This asymmetric response is not very surprising considering the

327   asymmetrical SST response. Nevertheless, the details of the teleconnection taking place in the

328   negative case are not fully understood but are beyond the scope of the present study.

329   Despite these significant impacts on T2M and tropical precipitations, no significant

330   impact could be identified on the major modes of atmospheric variability over the North

331   Atlantic sector, namely the North Atlantic Oscillation (NAO) and the East Atlantic Pattern

332   (not shown). The impact on the winter sea level pressure (SLP) pattern strongly varies with

333   the forecast range and a robust feature of the LOP impacts is difficult to identify at

334   interannual time scales (not shown). When averaging over the 5 to 10 forecast years, we find

335   a weak, but significant impact (Figure 4, 4th row) over various regions of the North Atlantic.

336   Again, the pattern of the impact differs between the positive and negative LOP. In N20, the

337   pattern has a significant positive anomaly over the Arctic and non-significant negative

338   anomalies over the North Atlantic mid-latitudes, which may be interpreted as a negative

339   NAO-like pattern. The SLP pattern identified for P20 exhibits a zonal dipole opposing the

340   northeastern coast of America with the southeastern European region. This structure does not

341   resemble any well-known patterns of large-scale atmospheric circulation variability from the

342   literature.

343

344

345   **4 Discussion: Impact on near term climate predictions**

346

347   In the previous section, it has been shown that the LOP - although computed from the

348   linear version of the oceanic component - successfully excites the subsurface variability mode

349   in the fully coupled system (i.e. the subsurface Rossby wave propagation and the associated

350   AMOC enhancement through thermal wind balance). Furthermore, it has been found that the

351   stimulation of this mode has a significant impact on the North Atlantic SST and some

352   atmospheric variables. However, this impact strongly depends on the magnitude of the LOP,

353   going from undetectable signal masked by the atmospheric stochastic noise (e.g. P01, P05) to

354   significant temperature anomalies over Europe during several years (P20). In this section, we

355   re-interpret the magnitude of the LOP in relation with the variability of the system, the

356   observational monitoring system in the real world, and a few other ensemble generation

357   strategies, in order to give a better insight of the potential usefulness of the LOP for

358   enhancing climate prediction reliability.

359

360   4.1 The LOP in the context of IPSL-CM5-LR internal variability

361   As mentioned in section 2, the magnitudes of the LOP tested in this study sample a

362   large fraction of the NAMT index variability in CTL. This is highlighted in Figure 6a, where

363   the colour points, indicating the NAMT value for the different magnitudes of the LOP, are

364 over-imposed on the grey shadings that represent respectively one, two, and three standard

365 deviations of NAMT interannual variability in CTL. We can see that P01 and P05 magnitudes

366 lie within one standard deviation of the variability from the mean state, which corresponds to

367 very frequent situations, while P20 and N20, on the other hand, rely within two and three

368 standard deviations, and therefore correspond to extreme, and relatively rare events. However,

369 the same analysis, repeated within 4 different oceanic layers (Figure 6b-e) highlights strong

370 discrepancies within the water column regarding this magnitude. Indeed, the LOP averaged

371 over the first 300 m on the same spatial domain ([30-70°N] in the Atlantic) are very weak

372 compared to the variability of the average temperature in the same layer in CTL (Figure 6b),

373 while they spread over a larger range of the variability in CTL in the deeper layers (Figure6d-

374 e). It is at intermediate depth, between 1000 and 2000m, that the range of LOP magnitudes

375 chosen here is the strongest as compared to the variability of the oceanic temperature in CTL,

376 (Figure 6d). Indeed, within this layer, the LOP strongest magnitude is around three standard

377 deviation of CTL. It could therefore be considered as an extreme event. In the assumption of a

378 normal distribution of the NAMT in that specific layer, the probability of such an event (P20

379 or N20) would be less that 1%.

380   This highlights that the complex 3D pattern of the LOP might create locally very large

381 perturbations as compared to the variability of the system, even though the strongest

382 magnitudes of the LOP are roughly co-located with the strongest temperature variability in

383 the North Atlantic found in CTL (Figure 1). To investigate the impact of such strong local

384 perturbations, we have generated an additional ensemble, referred to as P20MSK, and which

385 is similar to P20 but imposing a saturation of the perturbation pattern to 3 standard deviations

386 of the local variability in CTL. The magnitude of the perturbation of this new ensemble in

387 term of NAMT index is shown in Figure 6 as a black cross. The perturbation below 2000 m is

388 in particular considerably reduced, although it still reaches 3 standard deviations locally, as in

389 the eastern part of the basin in particular. In fact, this reduction of the spatial extent of the

390 LOP indeed does not affect significantly the response in terms of NAMT and AMOC

391 (Figure 2: *black crosses in right panels*). It therefore still stimulates the same Rossby wave

392 propagation mechanism. This suggests that the oceanic response to the LOP is not directly

393 due to its extreme integrated values but rather to its specifically located anomalies.

394

395   In summary, the LOPs exhibit a specific 3D pattern, with largest relative magnitudes

396 from intermediate to bottom depths, and a relatively weak perturbation at the surface, when

397 compared to the internal variability. Therefore, while occurrence of such anomalies is very

398 frequent at the surface for all magnitudes that we have tested, their occurrences are extremely

399 rare in the intermediate and deeper ocean. In that respect, P20 and N20 could be seen as

400 extreme events within the North-Atlantic Ocean. If a perturbation resembling the LOP was to

401 be detected, one could suspect – although based on this single coupled model analysis – an

402 AMOC anomaly after 5 years, followed by a NAMT anomaly and possible impacts over land,

403 which bring valuable information to assess the North-Atlantic climate a few years ahead. This

404 raises the question about the ability of current monitoring systems to detect such anomalies.

405 This is especially true for the eastern part of the deepest layer (below 2000 m), where the

406 perturbation is very strong, but lies below the maximum depth covered by current Argo floats.

407

408 4.2 The LOP in the context of oceanic initial state uncertainties in the real word

409

410 Here we compare the LOP to basic estimations of oceanic state error based on two

411 major data types commonly used to assess the oceanic state and variability: oceanic

412 reanalyses and the Argo float data (Figure 6, coral and green bars). Our first error estimation,

413 based on the reanalyses, consists in the integrated (NAMT spatial domain) annual mean

414 temperature differences between GLORYS and ORAS4 (Balmaseda et al., 2013). We chose

415 these reanalyses as they share the same ocean model (i.e. NEMO) as our coupled system

416 therefore facilitating the comparison on similar grids and tools. However, we reckon that this

417 choice likely tends to underestimate the real uncertainties acknowledged from the reanalysis

418 (e.g., Balmaseda et al. 2015; Palmer et al. 2015). The second error estimation, more directly

419 based on oceanic measurements uncertainty, uses the 2°-resolution temperature error field of

420 the objective interpolated Argo float dataset described in Desbruyères et al. (2016). Note that

421 to be comparable to the model analysis, both error estimations of the NAMT have been

422 rescaled by CTL variability. The detailed computation of these estimations, and their absolute

423 value (i.e., before rescaling) can be found in appendix 1 and 2. The two estimations give

424 different results, and this already highlights the complexity of assessing oceanic initial state

425 uncertainties and the large uncertainties that remain on these estimations. However, it gives

426 valuable information on the detectability of the LOP.

427 According to our estimation, in the upper ocean, even for the strongest LOP,

428 magnitudes tested here could not be separated from uncertainty of both reanalyses and Argo

429 data (Figure 6b). In contrast, in intermediate and deeper layers, highest magnitude LOPs can

430 be detected: below 1000 m, magnitudes of P10 or larger can be detected by both reanalyses

431 and Argo float datasets (only above 2000 m for the latter). Between 300 m and 1000 m, only

432 the largest magnitudes (i.e., P20 and N20) can be detected.

433   These results have strong implications for climate predictability, the LOP being a

434 source of predictability when detected by the observations. Indeed, in that case, the initial

435 conditions can be correctly assessed in order to phase the subsurface variability mode with the

436 observations resulting in the accurate prediction of its impacts on the surrounding climate. On

437 the other hand, for magnitudes lying under the detectability limit, the LOP's impact may help

438 anticipate uncertainties in climate predictions. These uncertainties could be decreased by

439 extending the monitoring system in the specific regions highlighted by the LOP pattern. In

440 particular, the ocean and the climate were shown to be strongly sensitive to anomalies located

441 below 2000 m, below the current depth of Argo float sampling. This suggests that the

442 deployment of deep Argo floats in the North Atlantic could lead to significant improvements

443 for decadal prediction skills for the North Atlantic region.

444   Note that the uncertainty estimation done here corresponds to the error on an annual

445 mean oceanic state, while the LOPs correspond to an instantaneous perturbation of the initial

446 state. However, persistence of the LOP can be seen from Figure 2b, where the initial

447 perturbation persists for more than one year before generating the anomaly response.

448 Therefore, although it is likely to underestimate the uncertainties on the instantaneous initial

449 state, this comparison still gives useful operational information.

450

451 4.3 The LOP for ensemble generation strategies

452   Taking into account the LOP in the prediction uncertainties can be achieved by

453 perturbing the initial state directly with the LOP to generate an ensemble. However, other

454 perturbation methods might take into account the uncertainty arising from the variability

455 mode associated to the LOP, depending on how the perturbation pattern projects onto the

456 LOP (Sévellec et al., *in rev*). Random perturbation of the 3D oceanic temperature field arising

457 from white noise local perturbations in each grid box - like used in Germe et al. (2017) -

458 rapidly goes to zero when averaged on a large spatial domain. Therefore, this method does not

459 adequately take into account possible deep density structures in the initial state uncertainties

460 and is likely to underestimate the ensemble spread arising from the subsurface variability

461 mode stimulated by the LOP. Another commonly used perturbation strategy of the ocean

462 initial state in near-term climate predictions is based on lagging the oceanic state by a few

463 days (e.g. Hazeleger et al., 2013). We have estimated the magnitude of such perturbations in

terms of NAMT using daily time series of the oceanic temperature in CTL. In practice, for each daily oceanic temperature pattern we have computed the anomaly from the oceanic temperature pattern occurring ten days before. Then, we compute the NAMT on these anomaly fields and take its minimum and maximum values as the range of the initial perturbations arising from this ensemble generation strategy. According to this analysis, the perturbation of the oceanic state due to a 10-day lagged temperature anomaly field is much larger in the surface layer (Figure 6b, *yellow bar*) than in the deeper layers where it remains very close to zero, especially bellow 2000 m (Figure 6e, *yellow bar*). This is consistent with the much stronger high frequency variability of the upper ocean. Therefore, the lagging methodology is very unlikely to generate perturbation patterns that project onto the LOP, and so to excite the subsurface variability mode.

Thus, generating decadal prediction ensemble through LOPs would sample a very different range of initial state uncertainties than other more traditional methods illustrated in Figure 6. Practically, this can be achieved by using LOPs of both signs, in addition to atmospheric perturbation for the ensemble generation. In this analysis, the ensemble resulting from merging N10 and P10 exhibits a larger ensemble spread than ATM for the forecast range near the maximal response to the LOP, i.e. 5 and 10 years for the AMOC and NAMT, respectively (not shown). However, this assessment is limited by the fact that the LOP is designed for a specific metric and a specific timescale. Therefore, an ensemble generation based on LOPs as defined in our study is only properly designed to create the largest ensemble spread for the AMOC and NAMT after 5 and 10 years, respectively. This might create an under- or overdispersive predictions regarding other metrics or time scales. This issue is shared with oceanic singular vectors ensemble generation, since the singular vectors also depends on a chosen norm and time scale. Marini et al. (2016) found that using oceanic singular vectors gives a better spread for locally assessed metrics during the first year as compared to atmospheric perturbations ensemble generation, while this spread is overestimated for integrated properties such as the AMOC or area-averaged SST. In their analysis, the 3D pattern of singular vectors used to generate the ensemble is not fully described at depth, but their Figure 3 shows local values of the initial ensemble spread around 0.25°C in the North-Atlantic at intermediate depth, which is comparable to our local values of interannual standard deviation in CTL. Therefore, prediction uncertainties arising from initial subsurface density uncertainties pattern as identified by the LOP are potentially taken into account by this method.

497

498

5 Conclusions

500

The impact of a linear optimal perturbation (LOP) of the 3D oceanic temperature field for the North Atlantic temperature and for large-scale circulation has been analysed based on a series of perfect model ensembles in the IPSL-CM5A-LR climate model. It has been found that the LOP, as identified in the adjoint version of the tangent linear model of the IPSL-CM5A-LR oceanic component, induces a similar response in terms of anomalous oceanic mean temperature and circulation than the linear forced ocean model. The response is nevertheless weaker (roughly by a factor 3) and occurs earlier than expected from the linear ocean model analysis. This can be explained by the non-linearities and damping terms from the ocean-atmosphere interactions, which were absent in the linear ocean model.

The computation of LOP in a fully coupled system would be very challenging. Indeed, computing the LOP in the forced ocean context enable to avoid atmospheric small-scale baroclinic instabilities and atmospheric convective instabilities. Within the linear framework used for computing LOP, such instabilities would not saturate and would dominate the solution. These small-scale instabilities would contaminate the large-scale response, preventing us to determine the climatically relevant large-scale solutions that we are aiming for. Still, despite the LOP based on the linear forced ocean model has a maximal signature at intermediate depths, it induces a strong SST change, hence leads to a significant impact on atmospheric surface temperature, precipitations, and to a lesser degree SLP at 5-10-year average forecast range. Even though our experimental design is idealized, these results have strong implications in terms of decadal predictability of the climate. Indeed, they highlight that anomalies in the deep ocean could have significant consequences for the upper ocean and surface atmosphere on timescales from interannual to decadal.

The impact of LOP on the oceanic heat content is rather linear, whereas the response of the SST and atmospheric variables are strongly asymmetric. Regarding the AMOC, its response exhibits a weak asymmetry. Although not significant in our case, this asymmetry has already been observed in the non-linear ocean forced model as a response to SSS optimal perturbations (Sévellec et al., 2008). As explained in Sévellec et al. (2008), this asymmetry may arise from the feedback of density anomalies on the vertical mixing. Indeed, a positive density anomaly will enhance the vertical mixing and therefore the deep-water formation, resulting in a stronger AMOC. On the other hand, a negative anomaly will reduce the vertical

531 mixing and the deep-water formation, resulting in a weaker AMOC. Depending on the
532 stratification before perturbation, the positive and negative perturbations will have a different
533 impact that may induce the asymmetry. Besides, even though we selected the initial state from
534 a neutral period regarding the NAMT and AMOC variability (cf. section 2), perfect neutrality
535 is elusive. Therefore, the asymmetry found in the response might result from the initial state
536 being closer to one sign version of the LOP than the other. Evaluating the impact of a peculiar
537 initial state on the AMOC response would require to test the LOP on several initial dates and
538 will be the object of future work. Likewise, even though an asymmetrical response of the
539 system to the LOP may arise from non-linear feedbacks or more generally from the non-linear
540 interaction of the stimulated linear response with other modes of variability or through non-
541 linear atmospheric and air-sea-ice interaction feedbacks, we cannot reach strong conclusions
542 from our experiments on that aspect.

543 The SST response to the positive LOP resembles a horseshoe pattern identified in both
544 the IPSL-CM5A-LR model and the observations by Gastineau et al. (2013) as influencing the
545 North Atlantic Oscillation (NAO) during the winter. It also resembles the North Atlantic
546 Multidecadal variability (AMV) pattern as identified in our coupled system (Gastineau et al.,
547 2013). The AMV, also known as the Atlantic Multidecadal Oscillation (AMO; Delworth et
548 al., 2007; Solomon et al., 2011), is known to influence the climate in the North Atlantic
549 region and in particular hurricanes activity (Goldenberg et al., 2011), and precipitations over
550 North America, Europe, and Sahel (Sutton and Hodson, 2005; Knight et al., 2006). A large
551 part of its influence over the Euro-Atlantic region seems to be related to its tropical
552 component with a weaker influence of the extratropical SST anomalies (Davini et al. 2015;
553 Peing et al., 2015). However, Gastineau et al. (2016) found a large oceanic influence of the
554 subpolar SST anomaly on the NAO in the IPSL-CM5A-LR model. While the SST pattern
555 associated with the LOP strongly resembles the SST anomaly pattern associated with a
556 negative NAO-like response in Gastineau et al. (2016), we could not identify a clear impact of
557 the LOP onto the NAO. This could come from a signal to noise ratio issue as 75-member
558 ensemble were used in their analysis, while we are using here 10 members at the most. This
559 highlights the complexity of the influence of the North Atlantic SST on the surrounding
560 climate. However, our results suggest that density anomalies in the deep North Atlantic could
561 be an oceanic decadal precursor for the AMV and its climatic consequences. This highlights
562 the potential of correct initialization of the full 3D oceanic state to improve climate
563 prediction.

564   Indeed, detecting such anomalies in the real deep ocean could provide a considerable
565   source of predictability, under the assumption that the modelled response in the atmosphere
566   presented here is representative of the real climate dynamics. The validity of this latter
567   assumption remains unclear given, for instance, that the response to an AMV-like pattern is
568   believed to be poorly simulated (Hodson et al. 2009). Upcoming CMIP6/DCPP simulations
569   (Boer et al. 2016) will allow to better evaluate the skill of new generation climate models to
570   represent such teleconnections between the Atlantic SST variations and the atmospheric
571   dynamics. Given the large impacts of the AMV inferred from statistical analysis of the
572   observations, it is possible that a better representation of these teleconnections in future
573   climate models could further enhance the potential climate impact and utility of a precise-
574   enough measurements of deep ocean anomalies.

575   A comparison of the LOP with an estimation of the oceanic state uncertainties based
576   on oceanic reanalyses and Argo float data reveals that even the largest magnitudes used here
577   cannot be detected by current monitoring systems in the upper ocean, where the perturbation
578   is the weakest. In contrast, in intermediate and deepest layers, the largest magnitudes (i.e. N20
579   and P20) stand out of the uncertainty range assessed by Argo float and reanalyses dataset,
580   suggesting that they could be detected by these observations and therefore initialized in
581   climate predictions. The fact that the largest amplitudes of the perturbation are found in the
582   deep ocean can be related with the larger persistence of such anomalies in the deeper ocean,
583   where they remain isolated from mean- and self-advection, as well as from the large mixing
584   induced by interactions with the atmosphere such as in the mixed layer. These anomalies are
585   able to persist over a sufficiently long time, maintaining meridional flow and amplifying the
586   transient change of the AMOC, which may explain why they are detected as optimal
587   perturbation for this circulation (cf. Sévellec and Fedorov 2015).

588   Our results also suggest that a climate prediction starting from an initial state
589   corresponding to an extreme event regarding the density anomaly in the deep North-Atlantic
590   would benefit from the initialization of the optimal structure determined in the ocean-only
591   model, therefore potentially increasing the prediction skill compared to the average skill in the
592   North-Atlantic region. On the other hand, if similar density anomalies are not detected in the
593   observations, they would become a substantial source of uncertainties that need to be taken
594   into account in climate prediction systems.

595

596

597   **Acknowledgments**

611

612

Appendix I: Estimates of oceanic state uncertainties from reanalyses

614

615   This estimation is based on GLORYS2V3 and ORAS4 (Balmaseda et al., 2013)

616   reanalyses. We computed the yearly NAMT and its layer components from both datasets over

617   the common period 1993-2014. Both reanalyses have been re-gridded on the ORCA2 grid to

618   share the exact same spatial and vertical domain for temperature average. These two time

619   series are then normalized and rescaled by CTL variability. Finally, the error estimation is

620   given by the root mean square error between these two time series.

621   This estimation is very likely to depend on the chosen reanalyses. The main objective is here

622   to give an order of magnitude of the differences between two state-of-the-art ocean

623   reanalyses.

624

Appendix II: Estimates of oceanic state uncertainties from ARGO floats data

626

627   We have used a 2° horizontal resolution x 20 db vertical resolution gridded

628   temperature and temperature error field based on the optimal interpolation of Argo float data.

629   The interpolation procedure is fully described in Desbruyères et al. (2016). This dataset

630   covers the 2000-2015 period, but we have restricted our analysis to the 2004-2015 period due

631   to non-representative poor sampling during the first years. We have computed the NAMT

632   index of the temperature field on raw data (Figure Ia: *black line*) and its annual mean (Figure

633   Ib: *black line*). The NAMT index computation can be written as:

634     $$NAMT = \sum_i w_i T_i \qquad (1)$$

635   Where T_i is the temperature in the grid cell i, and w_i is the weight related to the volume of the

636   grid cell i. The computation of the error on this index is based on the propagation of

637   uncertainties as described in Taylor et al. (1997). As the local errors δT_i cannot be considered

638   as independent, these local uncertainties induce further uncertainties on the NAMT index:

639    $$\delta NAMT \leq \sum_i w_i \delta T_i \qquad (2)$$

640   This error is shown in figure Ia as gray shading. This error estimation considers all grid cells

641   as dependant and therefore gives an upper bound of the error that is likely to overestimate the

642   real uncertainty.

643   When considering the annual means, the same propagation of error could be used.

644   However, this is very likely to strongly overestimate this uncertainty as the resulting error is

645   found to be larger than the variability of the NAMT index (Figure Ib: *gray shading*). In the

646   aim of giving more realistic error estimation, we have considered each realization as

647   independent for the computation of the annual mean. In that case, still following the

648   propagation of uncertainties described by Taylor et al. (1997), the error on the annual mean

649   NAMT can be written:

650    $$\langle \delta NAMT \rangle = \frac{1}{N_t} \sqrt{\sum_t \delta NAMT_t{}^2} \qquad (3)$$

651

652   Where N_t is the number of values in a given year. This more restrictive estimation is

653   highlighted in Figure Ib in red shading. In that case, considering each time step as

654   independent in a given year is a strong assumption that is likely to give an underestimation of

655   the uncertainties. This highlights the complexity of assessing the uncertainty on a regional

656   mean temperature from in situ measurement and the large remaining uncertainty on this

657   estimation. As this paper is not dedicated to the estimation of *in situ* measurement errors we

658   use the red shading estimation in the main paper, which appears as a reasonable assumption.

659   Finally, to compare the error estimation to the LOP in the context of the IPSL-CM5A-LR

660   variability we rescale this estimation by the variability in CTL. Therefore, the ARGO error

661   value used in Figure 2 is given by the following equation:

662

663    $$\sigma_{argo} = \frac{mean(\langle \delta NAMT \rangle)}{std(NAMT_{argo})} \times std(NAMT_{CTL}) \qquad (4)$$

664

665 Where $NAMT_{CTL}$ and $NAMT_{argo}$ are the annual time series of the NAMT index from CTL

666 and ARGO floats data respectively; $< \delta NAMT >$ is the error on $NAMT_{argo}$ (Figure Ib: *red*

667 *shading*).

668

669 **Table I**: Error on the layer components of NAMT from ARGO float dataset. The first column

670 corresponds to $mean(< \delta NAMT >)$ in equation (4), while the second column corresponds to

671 $\frac{mean(<\delta NAMT>)}{std(NAMT_{argo})}$ in (4).

	Raw error (in °C)	Normalized error
0-300m	0.036	0.32
300-1000m	0.038	0.53
1000-2000m	0.021	0.61

672

673

674

675 **References**

676

677 Aumont O and Bopp L (2006) Globalizing results from ocean in situ iron fertilization studies.

678 Glob Biogeochem Cycles 20, GB2017. doi: 10.1029/2005GB002591

679

680 Baehr J and Piontek R (2014) Ensemble initialization of the oceanic component of a coupled

681 model through bred vectors at seasonal- to-interannual timescales. Geosci Model Dev

682 7(1):453–461. doi:10.5194/gmd-7-453-2014

683

684 Balmaseda M A, Mogensen K, Weaver A (2013) Evaluation of the ECMWF Ocean

685 Reanalysis ORAS4. Q. J. R. Meteorol. Soc. doi:10.1002/qj.2063

686

687 Balmaseda M A, Hernandez F, Storto A, Palmer M D, Alves O, Shi L, Smith G C, Toyoda T,

688 Valdivieso M, Barnier B, Behringer D, Boyer T, Chang Y-S, Chepurin G A, Ferry N, Forget

689 G, Fujii Y, Good S, Guinehut S, Haines K, Ishikawa Y, Keeley S, Köhl A, Lee T, Martin M J,

690 Masina S, Masuda S, Meyssignac B, Mogensen K, Parent L, Peterson K A, Tang Y M, Yin Y,

691 Vernieres G, Wang X, Waters J, Wedd R, Wang O, Xue Y, Chevallier M, Lemieux J-F,

692 Dupont F, Kuragano T, Kamachi M, Awaji T, Caltabiano A, Wilmer-Becker K and Gaillard F

693   (2015) The Ocean Reanalyses Intercomparison Project (ORA-IP), Journal of Operational

694   Oceanography, 8:sup1, s80-s97, DOI: 10.1080/1755876X.2015.1022329

695

696   Boer, G.J. et al., 2016. The Decadal Climate Prediction Project (DCPP) contribution to

697   CMIP6. , pp.3751–3777.

698

699   Collins M, Botzet M, Carril AF, Drange H, Jouzeau A, Latif M, Masina S, Otteraa AH,

700   Pohlmann H, Sorteberg A, Sutton R, Terray L (2006) Interannual to decadal climate

701   predictabil- ity in the North Atlantic: a multimodel-ensemble study. J Clim 19(7):1195–1203.

702   doi:10.1175/JCLI3654.1

703

704   Collins, M and Sinha B (2003). Predictability of decadal variations in the thermohaline

705   circulation and climate. Geophys. Res. Let., 30(6), doi: 10.1029/2002GL016504

706

707   Desbruyères D G, E L McDonagh, B A King and V Thierry (2016) Global and Full-depth

708   Ocean Temperature Trends during the early 21st century from Argo and Repeat Hydrography.

709   J. Clim. doi: 10.1175/JCLI-D-16-0396.1

710

711   Dima M, and G Lohmann (2010) Evidence for Two Distinct Modes of Large-Scale Ocean

712   Circulation Changes over the Last Century", Journal of Climate, vol. 23, pp. 5-16,

713   doi:/10.1175/2009jcli2867.1

714

715   Doblas-Reyes F J, I Andreu_burillo, Y Chikamoto, J Garcia-Serrano, V Guemas, M Kimoto,

716   T Mochizuki, LRL Rodrigues and G J van Oldenborgh (2013) Initialized near-term

717   regional climate change prediction. Nat. Commun. 4, 1715, doi: 10.1038/ncomms2704

718

719   Du H, Doblas-Reyes FJ, García-Serrano J, Guemas V, Soufflet Y, Wouters B (2012)

720   Sensitivity of decadal predictions to the initial atmospheric and oceanic perturbations. Clim

721   Dyn, 39(7–8), 2013– 2023. doi:10.1007/s00382-011-1285-9

722

723   Dufresne JL, Foujols M-A, Denvil M-AS, Caubel A, Marti O, Aumont O, Balkanski Y, Bekki

724   S, Bellenger H, Benshila R, Bony S, Bopp L, Braconnot P, Brockmann P, Cadule P, Cheruy

725   F, Codron F, Cozic A, Cugnet D, de Noblet N, Duvel J-P, Ethé C, Fairhead L, Fichefet T,

726   Flavoni S, Friedlingstein P, Grandpeix J-Y, Guez L, Guilyardi E, Hauglustaine D, Hourdin F,

727   Idelkadi A, Ghattas J, Joussaume S, Kageyama M, Krinner G, Labetoulle S, Lahellec A,

728   Lefebvre M-P, Lefevre F, Levy C, Li ZX, Lloyd J, Lott F, Madec G, Mancip M, Marchand

729   M, Masson S, Meurdes- oif Y, Mignot J, Musat I, Parouty S, Polcher J, Rio C, Schulz M,

730   Swingedouw D, Szopa S, Talandier C, Terray P, Viovy N, Vuich- ard N (2013) Climate

731   change projections using the IPSL-CM5 Earth System Model: from CMIP3 to CMIP5. Clim

732   Dyn 40(9– 10):2123–2165. doi:10.1007/s00382-012-1636-1

733

734   Farrell, B. F. and Ioannou, P. J. (1996) Generalized stability theory. Part I: Autonomous

735   operators. J. of the Atmosph. sci., 53(14), 2025-2040.

736

737   Feng Q Y, and H A Dijkstra (2014). Are North Atlantic multidecadal SST anomalies

738   westward propagating?. Geophys. Res. Let., 41(2), 541-546.

739

740   Fichefet T, Maqueda MAM (1997) Sensitivity of a global sea ice model to the treatment of

741   ice thermodynamics and dynamics. J Geophys Res 102:2609–2612

742

743   Frankcombe L M, Dijkstra H A, and A. von der Heydt, 2008: Sub-surface signatures of the

744   Atlantic multidecadal oscillation. Geophys. Res. Lett., 35,L19602,

745   doi:10.1029/2008GL034989.

746

747   Gastineau G, D'Andrea F, and Frankignoul C (2013). Atmospheric response to the North

748   Atlantic Ocean variability on seasonal to decadal time scales. Clim. dyn., 40: 2311.

749   doi:10.1007/s00382-012-1333-0.

750

751   Gastineau G, L'hévéder B, Codron F, and Frankignoul C (2016). Mechanisms determining

752   the winter atmospheric response to the Atlantic overturning circulation. *J. of Clim.*, *29*(10),

753   3767-3785, doi: 10.1175/JCLI-D-15-0326.1

754

755   Germe A, Sévellec F, Mignot J, Swingedouw D and Nguyen S (2017) On the robustness of

756   near term climate predictability regarding initial state uncertainties. Clim. Dyn., 48(1-2),

757   353-366, doi:10.1007/s00382-016-3078-7

758

759   Griffies SM and Bryan K (1997) A predictability study of simulated North Atlantic

760   multidecadal variability. Clim Dyn 13(7–8):459– 487. doi:10.1007/s003820050177

761

762 Ham Y G, Rienecker M M, Suarez M J, Vikhliaev Y, Zhao B, Marshak J, Vernieres G and

763 Schubert S D (2014) Decadal prediction skill in the GEOS-5 forecast system. Clim. dyn.,

764 42(1-2), 1.

765

766 Hammer, G.L., J.W. Hansen, J.G. Phillips, J.W. Mjelde, H. Hill, A. Love, A. Potgieter (2001)

767 Advances in application of climate prediction in agriculture, Agricultural Systems, 70 (2-3),

768 p515-553, doi: http://dx.doi.org/10.1016/S0308-521X(01)00058-0

769

770 Hawkins E and R Sutton (2009) The potential to narrow uncertainty in regional climate

771 predictions. Bull. of the Am. Met. Soc., 90(8), 1095-1107.

772

773 Hazeleger W, Wouters B, Oldenborgh GJ, Corti S, Palmer T, Smith D, Storch JS (2013)

774 Predicting multiyear north atlantic ocean varia- bility. J Geophys Res 118(3):1087–1098.

775 doi:10.1002/jgrc.20117

776

777 Ho C K, Hawkins E, Shaffrey L, Broecker J, Hermanson L, Murphy J M, Smith D M and

778 Eade R (2013). Examining reliability of seasonal to decadal sea surface temperature forecasts:

779 The role of ensemble dispersion. Geophys. Res. Let., 40(21), 5770-5775,

780 10.1002/2013GL057630, 2013

781

782 Hourdin F, Foujols M-A, Codron F (2013) Impact of the LMDZ atmospheric grid

783 configuration on the climate and sensitiv- ity of the IPSL-CM5A coupled model. Clim Dyn.

784 doi:10.1007/ s00382-012-1411-3

785

786 Kirtman, B., S.B. Power, J.A. Adedoyin, G.J. Boer, R. Bojariu, I. Camilloni, F.J. Doblas-

787 Reyes, A.M. Fiore, M. Kimoto, G.A. Meehl, M. Prather, A. Sarr, C. SchaÅNr, R. Sutton, G.J.

788 van Oldenborgh, G. Vecchi and H.J. Wang, (2013) Near-term Climate Change: Projections

789 and Predictability. In: Climate Change 2013: The Physical Science Basis. Contribution of

790 Working Group I to the Fifth Assessment Report of the Intergovernmental Panel on Climate

791 Change [Stocker, T.F., D. Qin, G.-K. Plattner, M. Tignor, S.K. Allen, J. Boschung, A. Nauels,

792 Y. Xia, V. Bex and P.M. Midgley (eds.)]. Cambridge University Press, Cambridge, United

793 Kingdom and New York, NY, USA.

794

795 Knight JR, Folland CK, Scaife AA (2006) Climate impacts of the Atlantic multidecadal
796 oscillation. Geophys Res Let 33:L17706. doi:10.1029/2006GL026242

797

798 Madec G (2008) NEMO ocean engine, Technical note, IPSL. Avail- able at
799 http://www.nemo-ocean.eu/content/download/11245/560 55/file/NEMO_book_v3_2.pdf

800

801 Marini C, Polkova I, Köhl A, and Stammer D (2016) A comparison of two ensemble
802 generation methods using oceanic singular vectors and atmospheric lagged initialization for
803 decadal climate prediction. *Month. Weath. Rev., 144*(7), 2719-2738, doi: 10.1175/MWR-D-
804 15-0350.1.

805

806 Meehl, G. A., et al. (2013) Decadal climate prediction: An update from the trenches. Bull.
807 Am. Met. Soc., doi:10.1175/BAMS-D-12-00241.1.

808

809 Mignot J, Garcia-Serrano J, Swingedouw D, Germe A, Nguyen S, Ortega P, Guilyardi E, Ray
810 S (2016) Decadal prediction skill in the ocean with surface nudging in the IPSL-CM5A-LR
811 climate model. Clim Dyn. doi:10.1007/s00382-015-2898-1

812

813 Mignot J, Swingedouw D, Deshayes J, Marti O, Talandier C, Séférian R, Lengaigne M,
814 Madec G (2013) On the evolution of the oceanic component of the IPSL climate models from
815 CMIP3 to CMIP5: a mean state comparison. Ocean Model 72:167–184.
816 doi:10.1016/j.ocemod.2013.09.001

817

818 Muir L C and Fedorov A V (2016) Evidence of the AMOC interdecadal mode related to
819 westward propagation of temperature anomalies in CMIP5 models. Clim. Dyn., 1-19.
820 doi:10.1007/s00382-016-3157-9

821

822 Hodson, D. L. R., Sutton, R., Cassou, C., Keenlyside, N., Okumura, Y. and Zhou, T. (2009)
823 *Climate impacts of recent multidecadal changes in atlantic ocean sea surface temperature: a*
824 *multimodel comparison*, Climate Dynamics, doi:10.1007/s00382-009-0571-2

825

826 Ortega P, Mignot J, Swingedouw D, Sévellec F, Guilyardi E (2015) Reconciling two
827 alternative mechanisms behind bi-decadal variability in the North Atlantic. Prog Oceanogr
828 137:237–249. doi:10.1016/j.pocean.2015.06.009

829

830　Ortega P, Guilyardi E, Swingedouw D, Mignot J, and Nguyen S (2017). Reconstructing

831　extreme AMOC events through nudging of the ocean surface: a perfect model approach.

832　*Clim. Dyn*, doi: 10.1007/s00382-017-3521-4.

833

834　Palmer, T N, Buizza R, Hagedorn R, Lawrence A, Leutbecher M and Smith L (2006)

835　Ensemble prediction: a pedagogical perspective. ECMWF Newsletter 106, 10–17.

836

837　Palmer T N, and Zanna L (2013) Singular vectors, predictability and ensemble forecasting for

838　weather and climate. *Journal of Physics A: Mathematical and Theoretical*, *46*(25), 254018,

839　10.1088/1751-8113/46/25/254018

840

841　Palmer M D, Roberts C D, Balmaseda M, Chang Y-S, Chepurin G, Ferry N, Fujii Y, Good

842　SA, Guinehut S, Haines K, Hernandez F, Köhl A, Lee T, Martin M J, Masina S, Masuda S,

843　Peterson K A, Storto A, Toyoda T, Valdivieso M, Vernieres G, Wang O and Xue Y (2015)

844　Ocean heat content variability and change in an ensemble of ocean reanalyses. Clim. Dyn.,

845　doi:10.1007/s00382-015-2801-0

846

847　Persechino A, Mignot J, Swingedouw D, Labetoulle S, Guilyardi E (2013) Decadal

848　predictability of the Atlantic meridi- onal overturning circulation and climate in the IPSL-

849　CM5A- LR model. Clim Dyn 40(9–10):2359–2380. doi:10.1007/ s00382-012-1466-1

850

851　Pohlmann H, Botzet M, Latif M, Roesch A, Wild M, Tschuck P (2004) Estimating the

852　decadal predictability of a coupled AOGCM. J Clim 17(22):4463–4472. doi:10.1175/3209.1

853

854　Ray S, Swingedouw D, Mignot J, Guilyardi E (2014) Effect of sur- face restoring on

855　subsurface variability in a climate model during 1949–2005. Clim Dyn. doi:10.1007/s00382-

856　014-2358-3

857

858　Romanova V and Hense A (2015) Anomaly transform methods based on total energy and

859　ocean heat content norms for generating ocean dynamic disturbances for ensemble climate

860　forecasts. Clim Dyn. doi:10.1007/s00382-015-2567-4

861

862   Servonnat J, Mignot J, Guilyardi E, Swingedouw D, Séférian R, Labetoulle S (2014)

863   Reconstructing the subsurface ocean dec- adal variability, using surface nudging in a perfect

864   model frame- work. Clim. Dyn. doi:10.1007/s00382-014-2184-7

865

866   Sévellec F, Fedorov AV (2017) Predictability and decadal variability of the North Atlantic

867   ocean state evaluated from a realistic ocean model. J. Clim., 30(2):477-498., doi:

868   10.1175/JCLI-D-16-0323.1

869

870   Sévellec F, Fedorov AV (2015) Optimal excitation of AMOC decadal variability: Links to the

871   subpolar ocean. Prog. in Oceanogr. 132:287-304.

872   doi: http://dx.doi.org/10.1016/j.pocean.2014.02.006

873

874   Sévellec F and Huck T (2015) Theoretical investigation of the Atlantic multidecadal oscil-

875   lation. J. Phys. Oceanogr., 45, 2189–2208.

876

877   Sévellec F, Fedorov AV (2013a) Model bias reduction and the limits of oceanic decadal

878   predictability: importance of the deep ocean. J. Clim. 26(11):3688–3707. doi:10.1175/JCLI-

879   D-12-00199.1

880

881   Sévellec F, Fedorov AV (2013b) The Leading, interdecadal eigonmode of the Atlantic

882   Meridional Overturning circulation in a realistic ocean model. J. Clim. 26:2160-2183.

883   doi:10.1175/JCLI-D-11-00023.1

884

885   Sévellec F, Huck T, Ben Jelloul M, Grima N, Vialard J and Weaver A (2008) Optimal surface

886   salinity perturbations of the meridional overturning and heat transport in a global ocean

887   general circulation model. J. Phys. Oceanogr. 38(12): 2739-2754.

888   doi:10.1175/2008JPO3875.1

889

890   Sévellec F, M B Jelloui and T Huck (2007) Optimal surface salinity perturbations influencing

891   the thermohaline circulation. J. Phys. Oceanogr. 37(12): 2789-2808. doi:

892   10.1175/2007JPO3680.1

893

894   Slingo J and T N Palmer (2011) Uncertainty in weather and climate prediction. Phil. Trans.

895   Roy. Soc. A 369, 4751–4767. doi:10.1098/rsta.2011.0161

896

897 Solomon A, and Coauthors, (2011) Distinguishing the roles of natural and anthropogenically
898 forced decadal climate variability. Bull. Amer. Meteor. Soc., 92, 141–156.

899

900 Stan C and Kirtman B P (2008) The influence of atmospheric noise and uncertainty in ocean
901 initial conditions on the limit of predictability in a coupled GCM. J Clim 21(14):3487–3503.
902 doi:10.1175/20 07JCLI2071.1

903

904 Swingedouw D, Mignot J, Labetoulle S, Guilyardi E, Madec G (2013) Initialisation and
905 predictability of the AMOC over the last 50 years in a climate model. Clim Dyn 40(9–
906 10):2381–2399. doi:10.1007/s00382-012-1516-8

907

908 Taylor J R (1997) An Introduction to Error Analysis, 2nd edition, Sausalito, CA. University
909 Science Books, 327 pp.

910

911 Tulloch R, Marshall J, and Smith K S (2009). Interpretation of the propagation of surface
912 altimetric observations in terms of planetary waves and geostrophic turbulence. J. of
913 Geophys. Res.: Oceans, 114(C2).

914

915 Valcke S (2006) OASIS3 user guide (prism_2-5), technical report TR/ CMGC/06/73, PRISM
916 report no 2. CERFACS, Toulouse, p 60

917

918 Vianna M L, and Menezes V V (2013). Bidecadal sea level modes in the North and South
919 Atlantic Oceans. Geophys. Res. Let., 40(22), 5926-5931.

920

921 Yeager S, Karspeck A, Danabasoglu G, Tribbia J, and Teng H (2012) A decadal prediction
922 case study: Late twentieth-century North Atlantic Ocean heat content. J. of Clim., 25(15),
923 5173-5189, doi: 10.1175/JCLI-D-11-00595.1

924

925 Zanna L, Heimbach P, Moore A M, and Tziperman E (2011) Optimal excitation of
926 interannual Atlantic meridional overturning circulation variability. J. of Clim., 24(2), 413-
927 427, doi: 10.1175/2010JCLI3610.1.

928

929

930   Table 1: Summary of the characteristics of the ensembles.

	Oceanic perturbation factor	*Number of members*	*Start date*	*Length*
ATM	0	10	1st of January 1991	20 years
P01	1	5	-	-
P05	5	5	-	-
P10	10	5	-	-
P20	20	10	-	-
N10	-10	5	-	-
N20	-20	10	-	-

931

932

Figure 1

Colours shading: The spatial structure of the imposed linear optimal temperature

perturbations (LOP, in °C) at the ocean surface (*top left panel*), and at 217 m (*top right*

panel), 1033 m (*bottom left panel*) and 2768 m (*bottom right panel*). The amplitudes shown

here correspond to the original LOP, i.e. scaled by a factor of 1 (see text for details). Black

contours indicate interannual standard deviation of local ocean temperature in the 1000-year

long CTL simulation at these depths. The contours are spaced by 0.4°C within the range from

0.4 to 2°C at the surface and at 217 m depth, by 0.1°C from 0.1 to 0.5°C at 1033 m, and by

0.02°C from 0.02°C to 0.12°C at 2768 m.

942

943

944

945

946
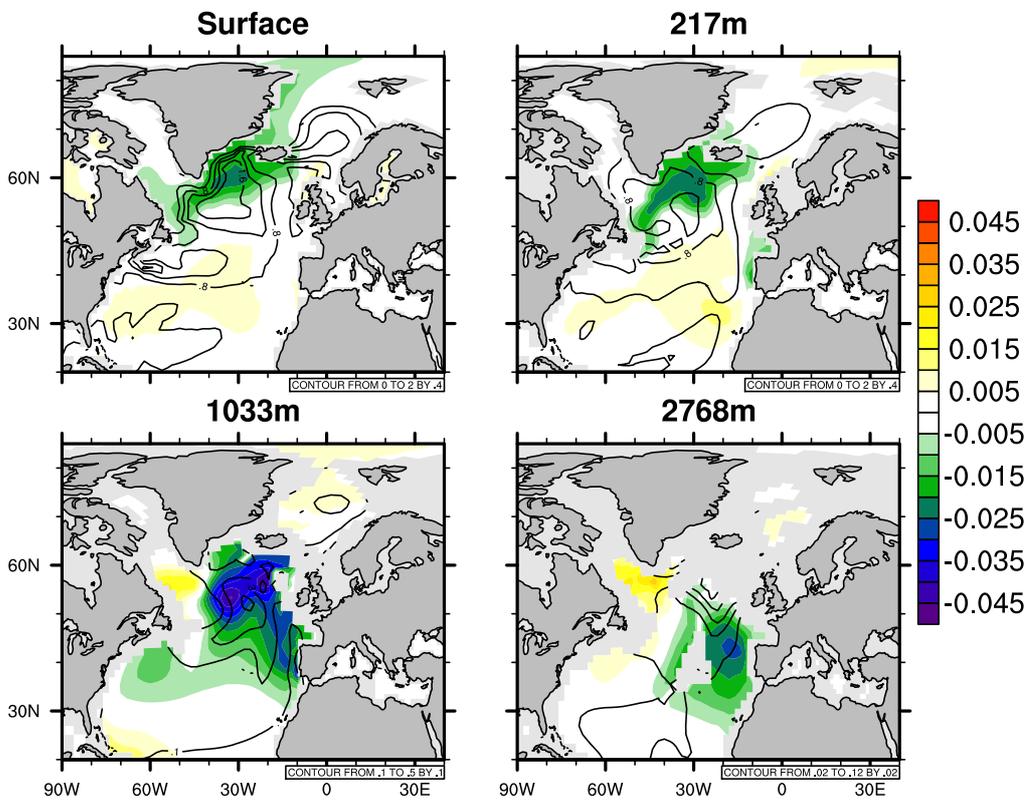
Figure 2

948 *Left and middle panels*: The response of NAMT (*top*) and AMOC (*bottom*) to the imposed

949 perturbation for different LOPs' amplitudes (colours). The time evolution of the ensemble

950 mean for all the experiments are shown on the left panel while the middle panel highlights the

951 99% confidence interval of the ensemble mean for P20 (*red line*), N20 (*blue line*), and ATM

952 (*grey line*). The *vertical black line* in middle panel highlights the date at which the magnitude

953 of the response has been assessed to draw the right panels. It corresponds to a 10-year forecast

954 for the NAMT (top) and 5-year forecast for the AMOC (bottom). Time axes refer to model

955 years. *Right panels*: Magnitude of the NAMT (*top*) and AMOC (*bottom*) response as a

956 function of the magnitude of the perturbation at 10- and 5-year forecast range, respectively.

957 Error bars correspond to the ensemble mean 99%-level confident interval. The *solid black line*

958 shows the best linear fit. The *gray shading* in the top panel indicates the response magnitude

959 as expected from the linear model as described by Sévellec and Fedorov (2017).

960

961

962
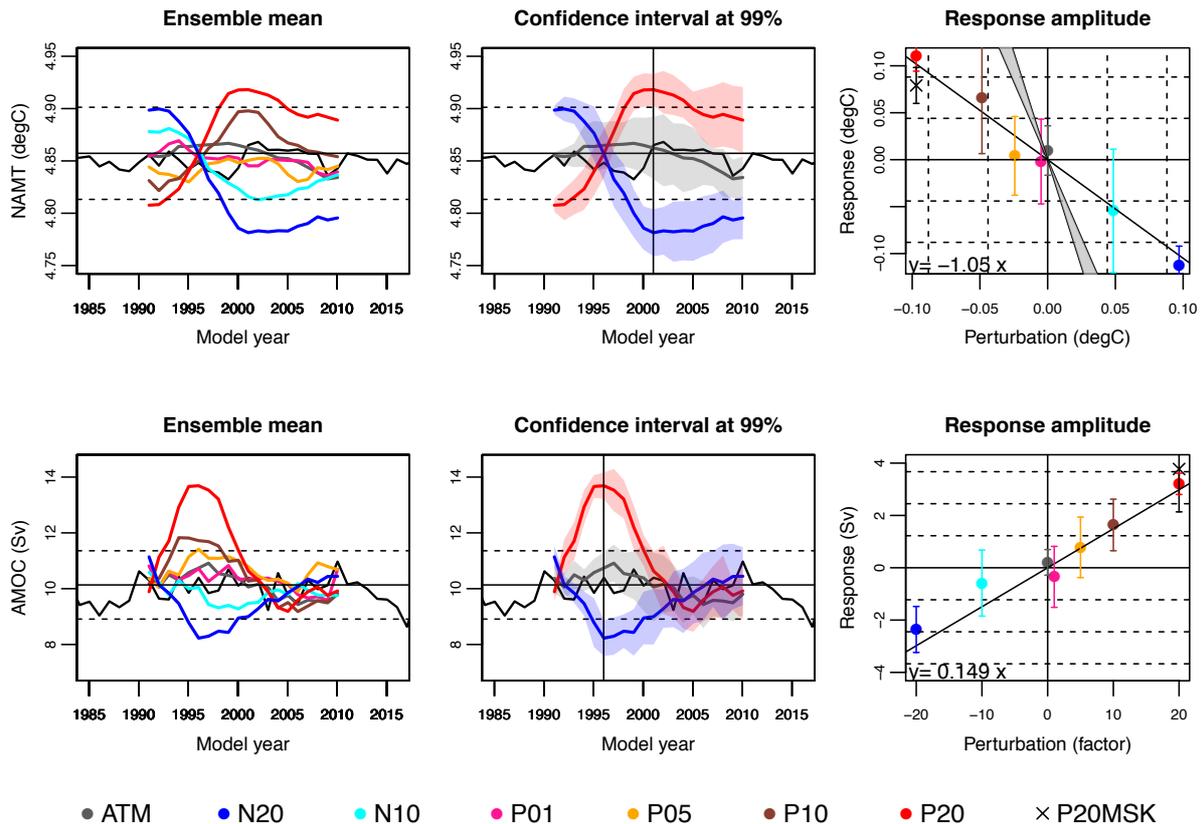
Figure 3

Left top panel: Ensemble mean time evolution of the NAMT300 for P20 (*red*), N20 (*blue*), and ATM (*gray*) ensembles. The *Shading* highlights the confident interval on the ensemble mean according to a t-test at the 99% level. Time axis refers to model years. The *black curve* corresponds to the time series of this index in CTL simulation with black dashed lines indicating ± 1 standard deviation. The *black vertical bars* indicate the selected years mapped in middle and right panels.

Left bottom panel: Correlation map between annual T300 at each grid point and the AMOC index in the CTL simulation. *Black dots* highlight correlations significant at the 95% level.

Middle and right panels: T300 differences (in colour) between P20 ensemble mean and ATM ensemble mean at 1-year (*top middle panel*), 5-year (*top right panel*), 10-year (*bottom middle panel*), and 15-year (*bottom right panel*) forecast range. Differences are expressed in °C. The background T300 climatology field in CTL is represented in *black contours*. The line contour interval is 2.5°C. *Horizontal red lines* highlight the 30 and 70°N latitude, i.e. the zonal boundaries of the NAMT index. *Black dots* highlight the areas where the plotted ensemble mean is significantly different from ATM ensemble mean at 95% level.
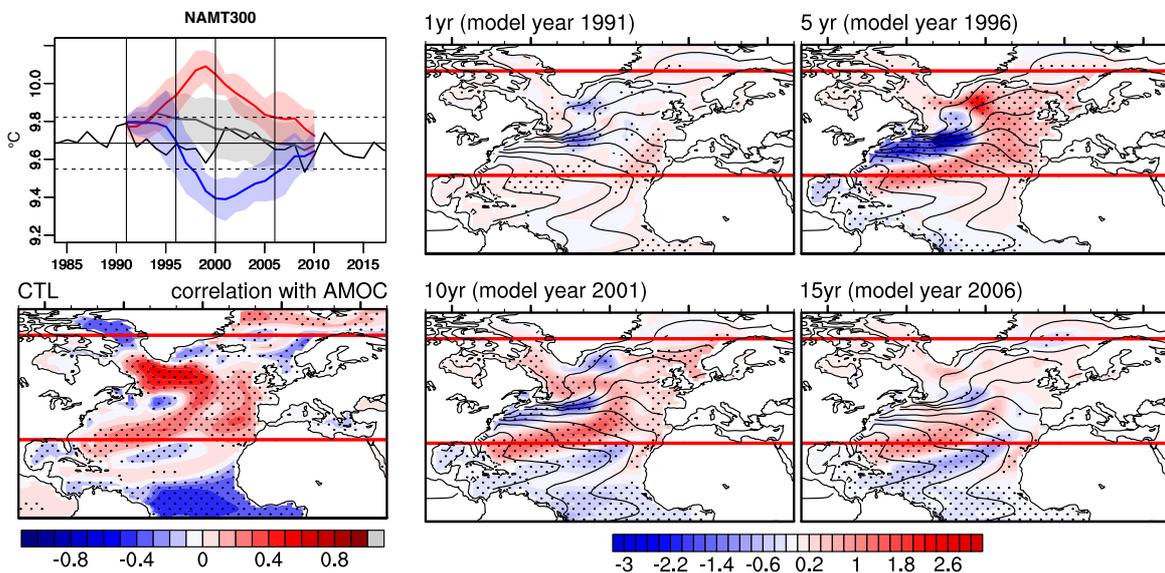
Figure 4

SST differences of N20 (*left panels*) and P20 (*right panels*) ensemble mean with respect to ATM ensemble mean averaged over 5-year to 10-year forecast range. Differences are drawn for annual mean SST in °C (*1st row*), annual mean T2M in °C (*2nd row*), summer seasonal mean (June to August) precipitation in kg s^{-1} m^{-2} (*3rd row panels*) and winter (January to March) sea level pressure in hPa (*4th row*). *Black dots* highlight the areas where N20 or P20 ensemble means are significantly different from ATM ensemble mean at the 95% level.
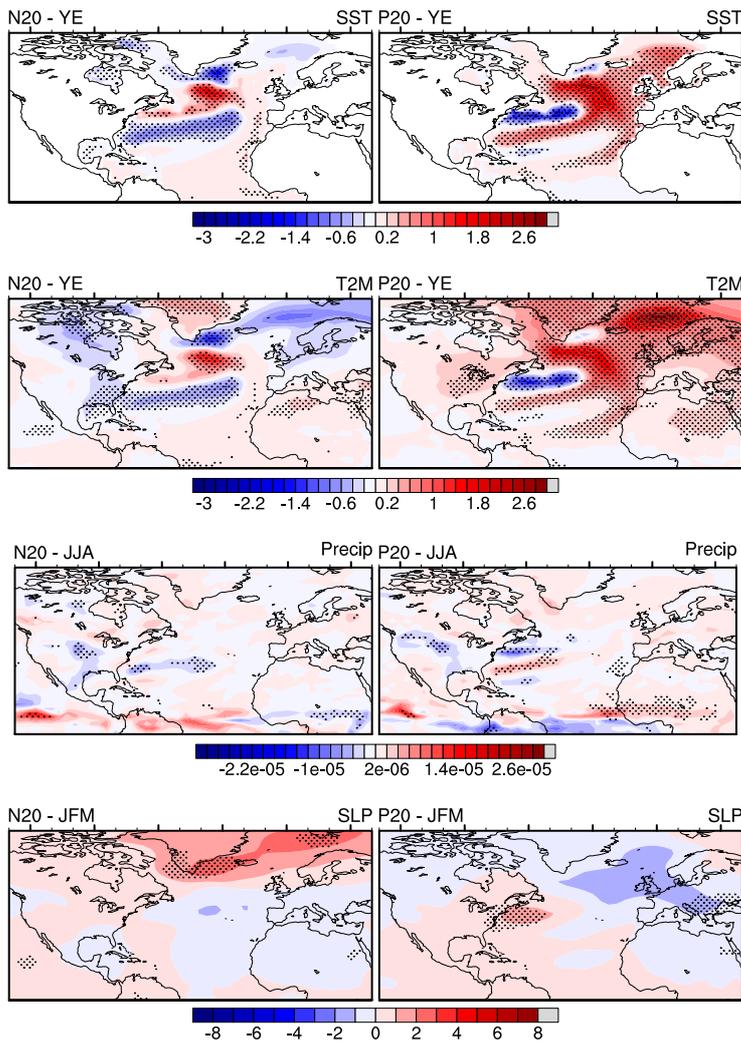
994 **Figure 5**

995 T2M differences of P20 ensemble mean with respect to ATM ensemble mean for 5-year to

996 10-year forecast range. Differences are drawn for winter (January to March, *left panels*) and

997 summer (June to August, *right panels*) mean surface air temperature in °C. *Black dots*

998 highlight the areas where P20 ensemble mean is significantly different from ATM ensemble

999 mean at the 95% level.
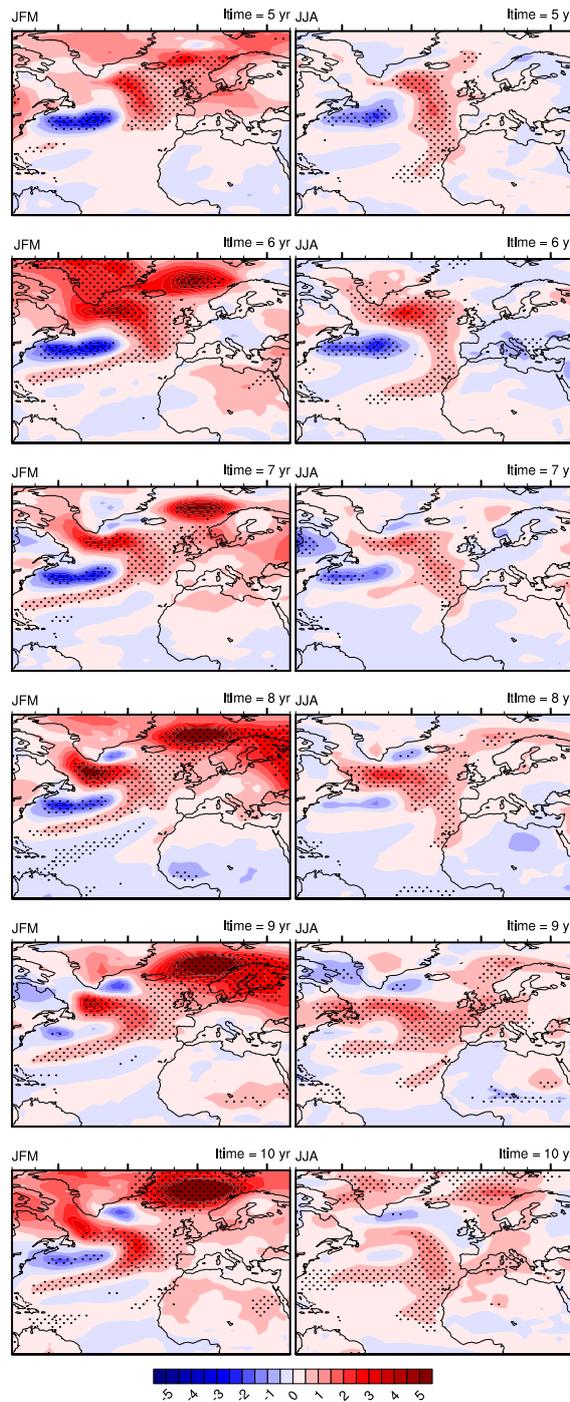
1000
1001

Figure 6

1003 (a) NAMT and its vertical contributions within layers (b) 0-300 m, (c) 300-1000 m, (d) 1000-

1004 2000 m, and (e) below 2000 m of: the LOPs (LOP, *color points and black crosses*), 10-day

1005 lagged perturbation patterns (LAG; range in *yellow bars*), an uncertainty estimation based on

1006 reanalyses (REA; range in *coral bars*), and an Argo float uncertainty (ARGO; *light green*

1007 *bars*). Note that there is no ARGO estimation in (e), as ARGO floats only sample the water

1008 column above 2000 m. *Gray shadings* indicate ±1, ±2, and ±3 interannual standard deviations

1009 of the same indices in CTL.
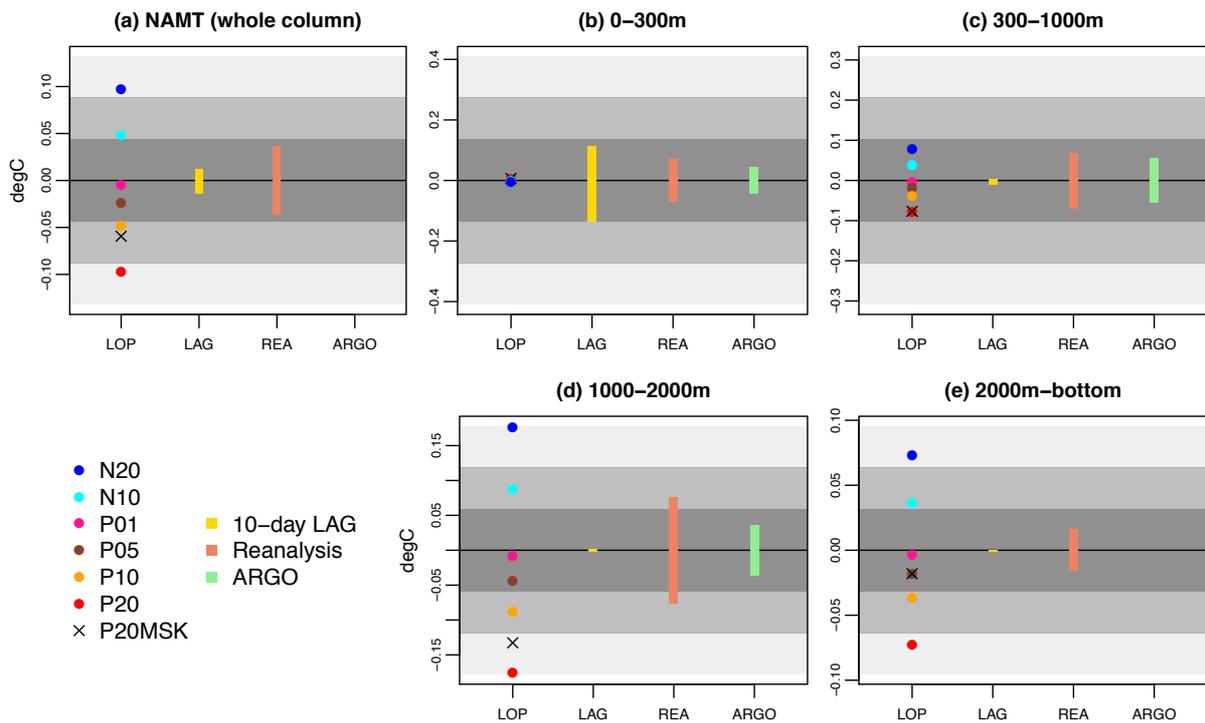
1010
1011
1012
1013
1014
1015
1016
1017
1018
1019
1020
1021

Figure I

NAMT index based on Argo float dataset (surface to 2000m) from (a) 10-day average data

and (b) annual means. The *gray shading* gives the upper bound of the error based on Taylor et

al. (1997). The *red shading* gives the annual mean error estimation of the error when

considering the time-steps within a year as independent.

Figure 1

Surface

217m

1033m

2768m

CONTOUR FROM 0 TO 2 BY .4

CONTOUR FROM 0 TO 2 BY .4

CONTOUR FROM .1 TO .5 BY .1

CONTOUR FROM .02 TO .12 BY .02

60N

30N

60N

30N

90W   60W   30W   0   30E

90W   60W   30W   0   30E

0.045
0.035
0.025
0.015
0.005
-0.005
-0.015
-0.025
-0.035
-0.045

Figure 2

Figure 3

NAMT300
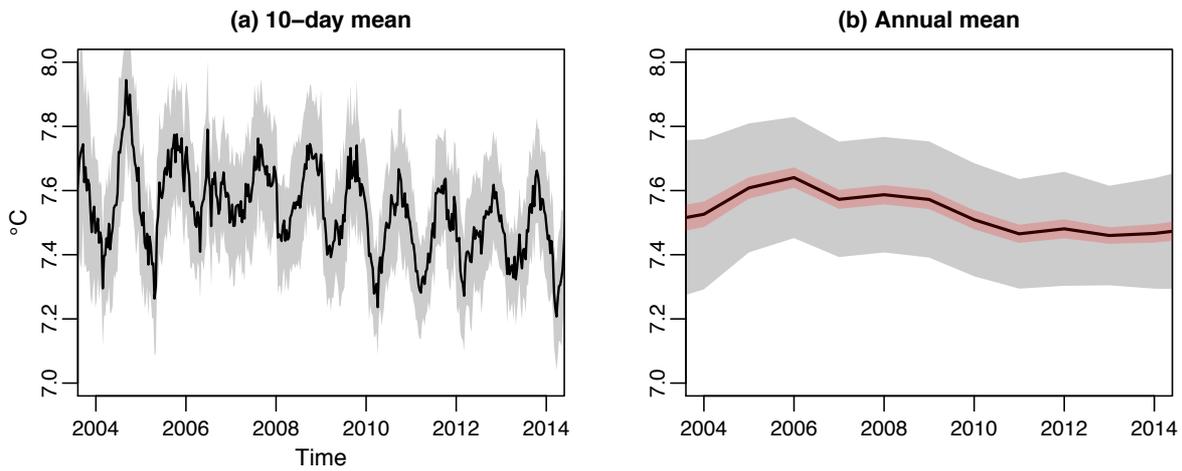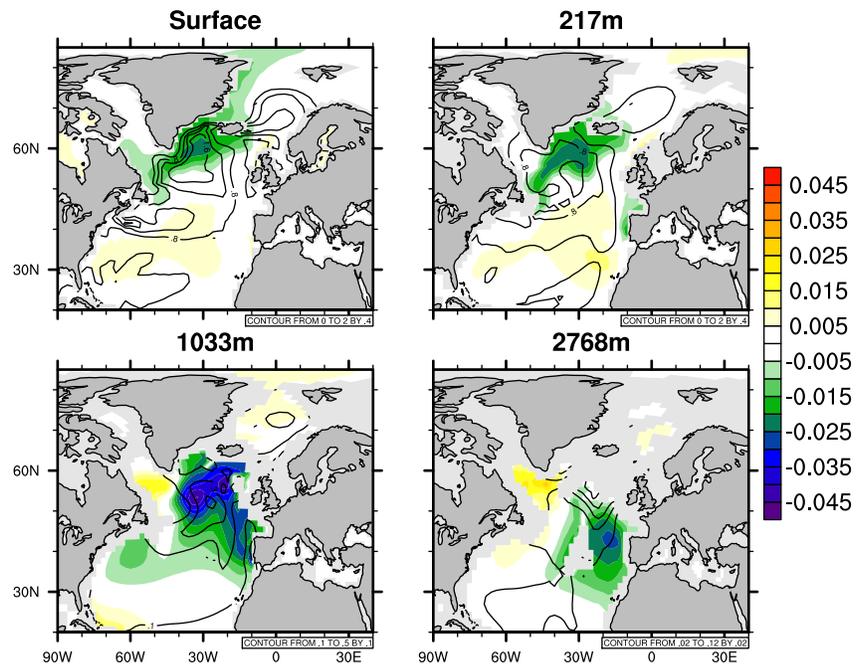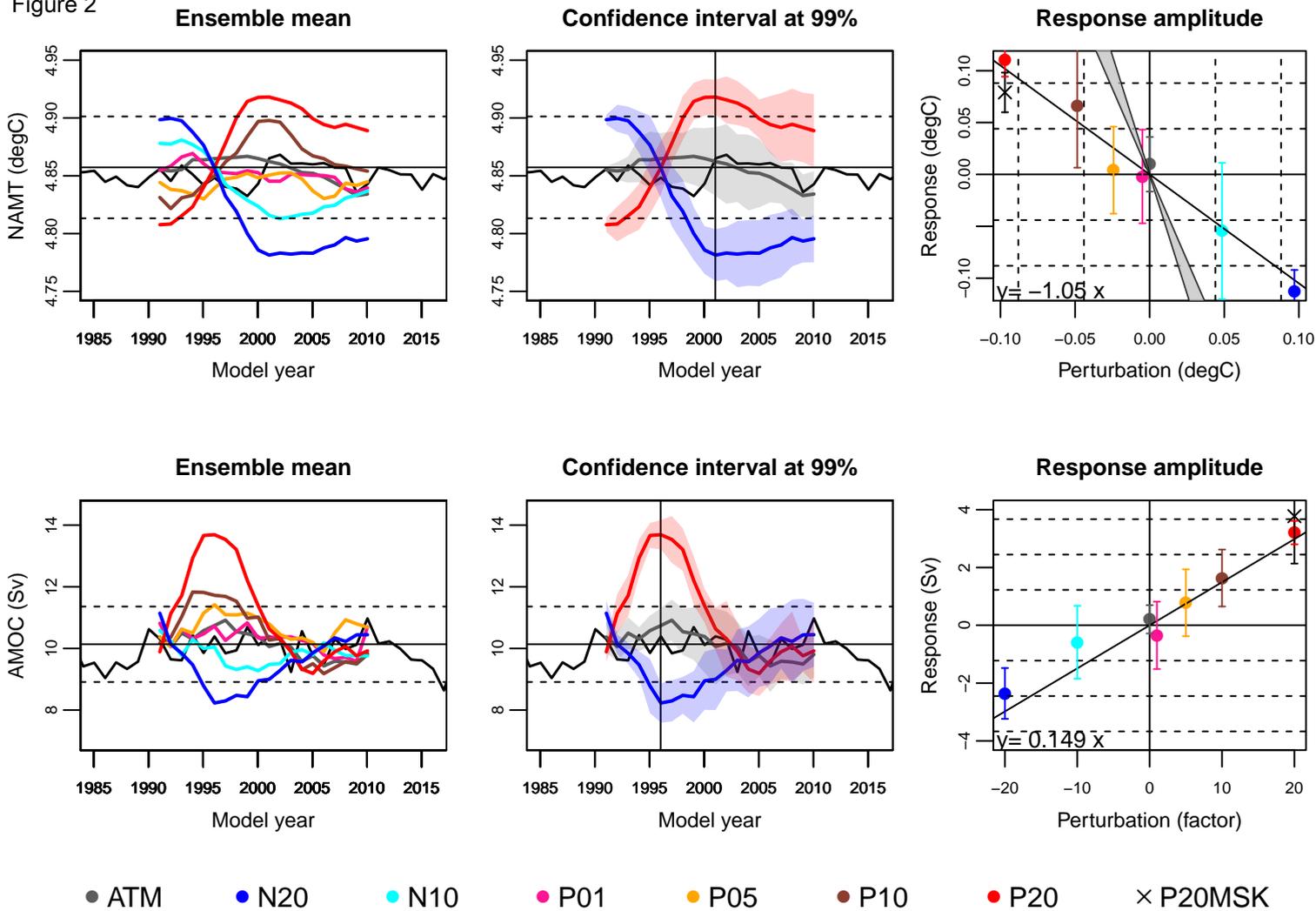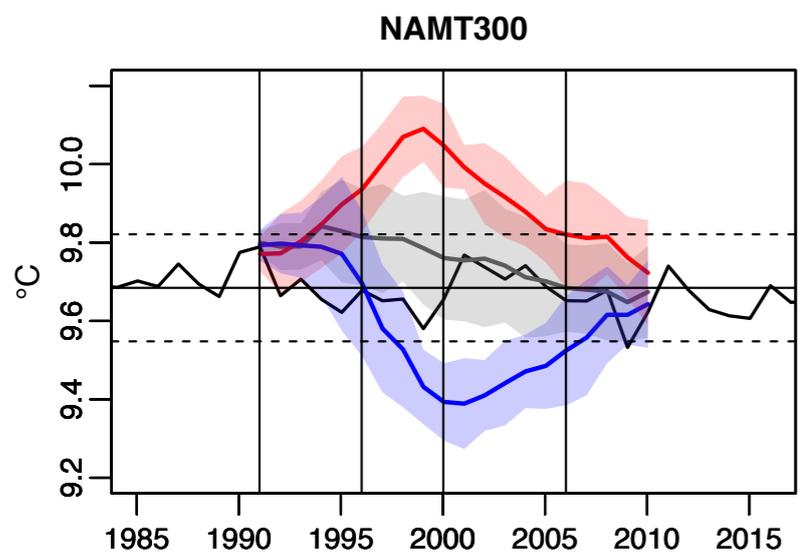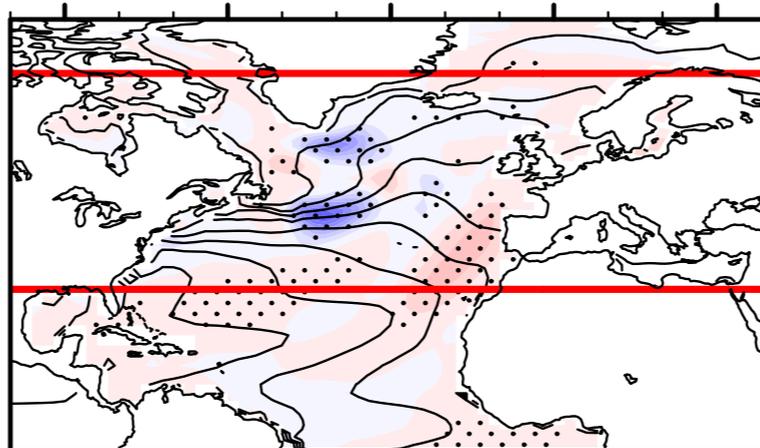
1yr (model year 1991)

5 yr (model year 1996)
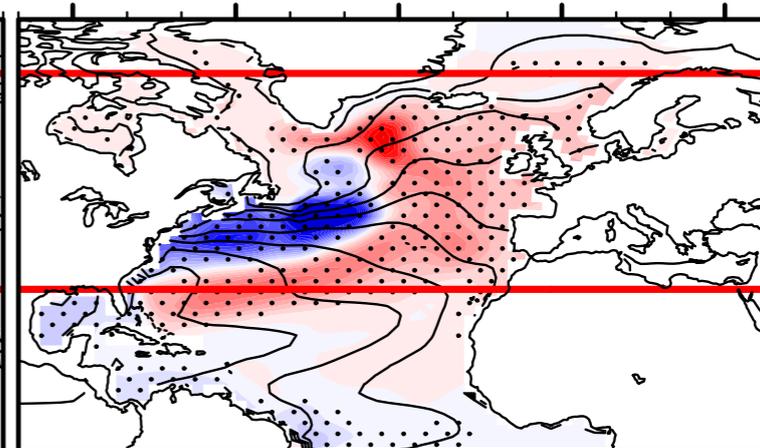
CTL   correlation with AMOC
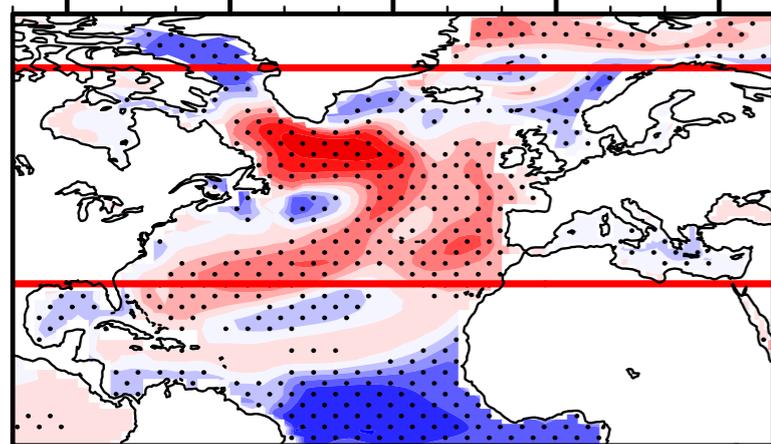
10yr (model year 2001)
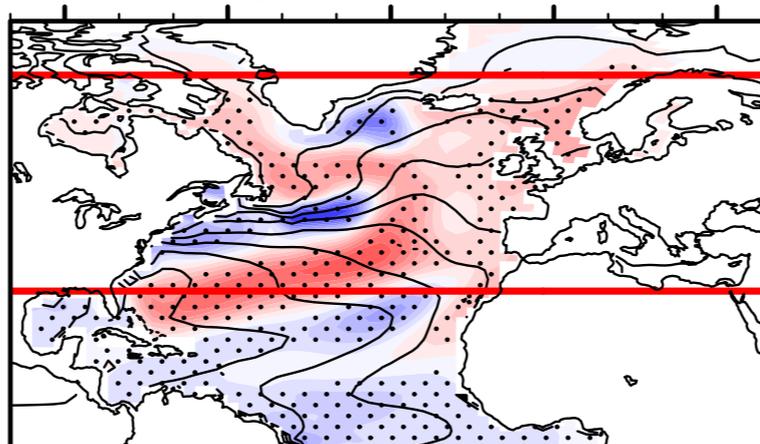
15 yr (model year 2006)
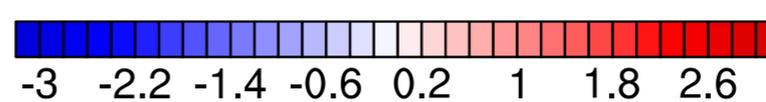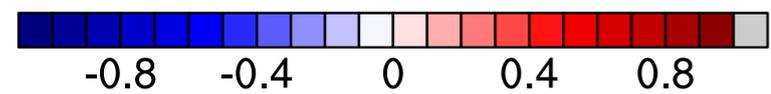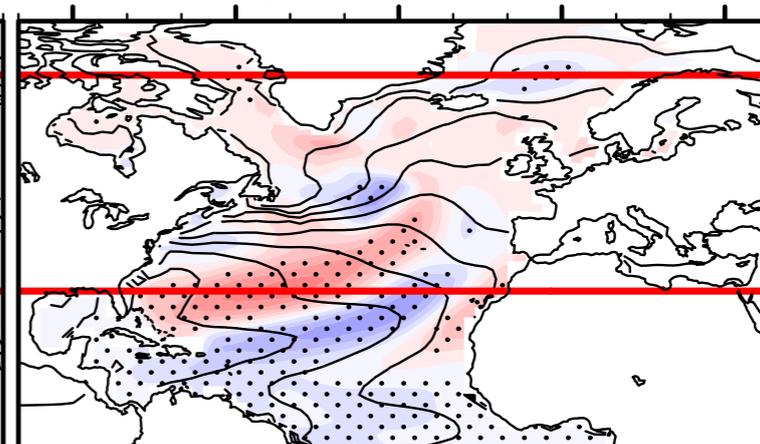
Figure 4
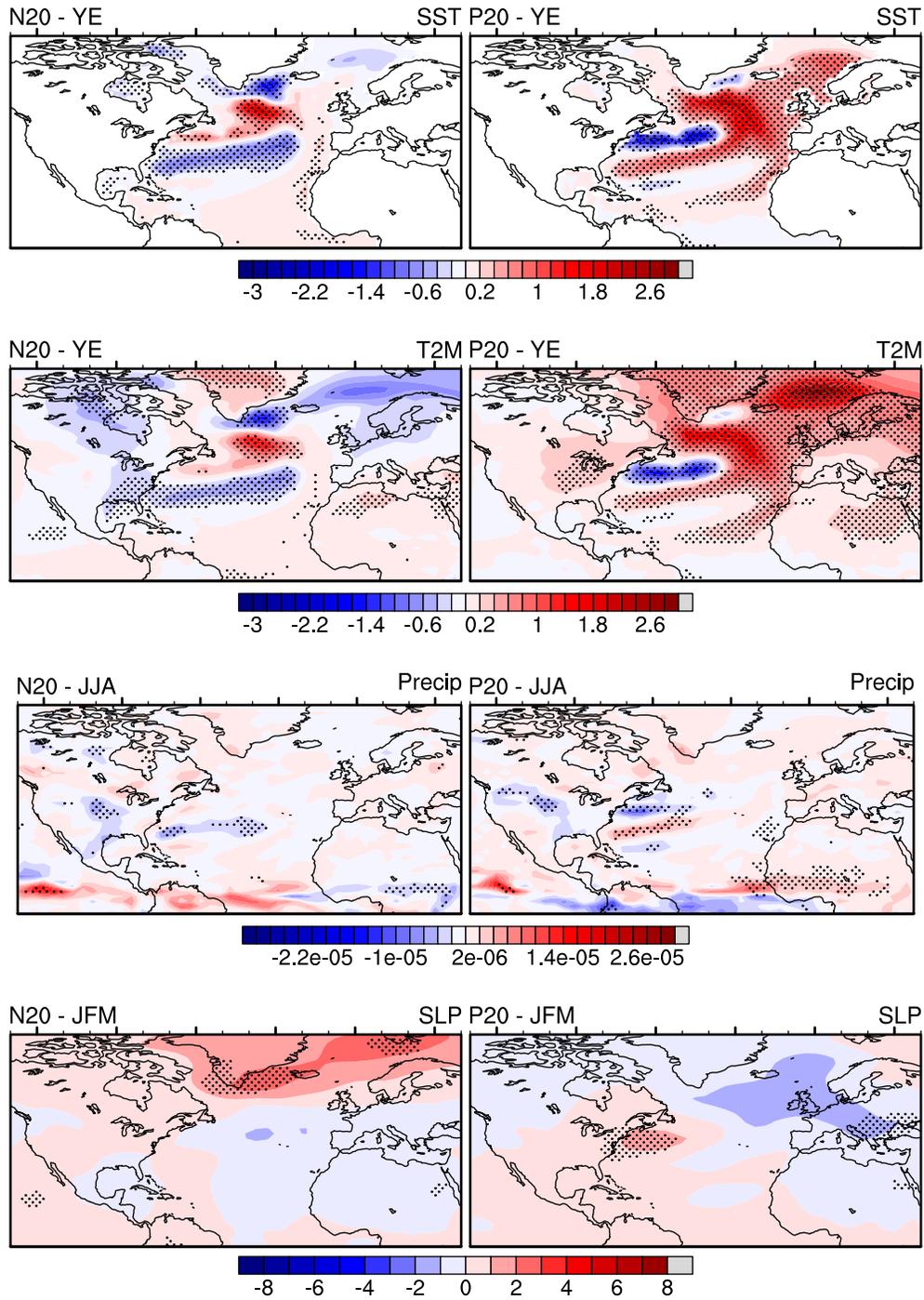
Figure 5
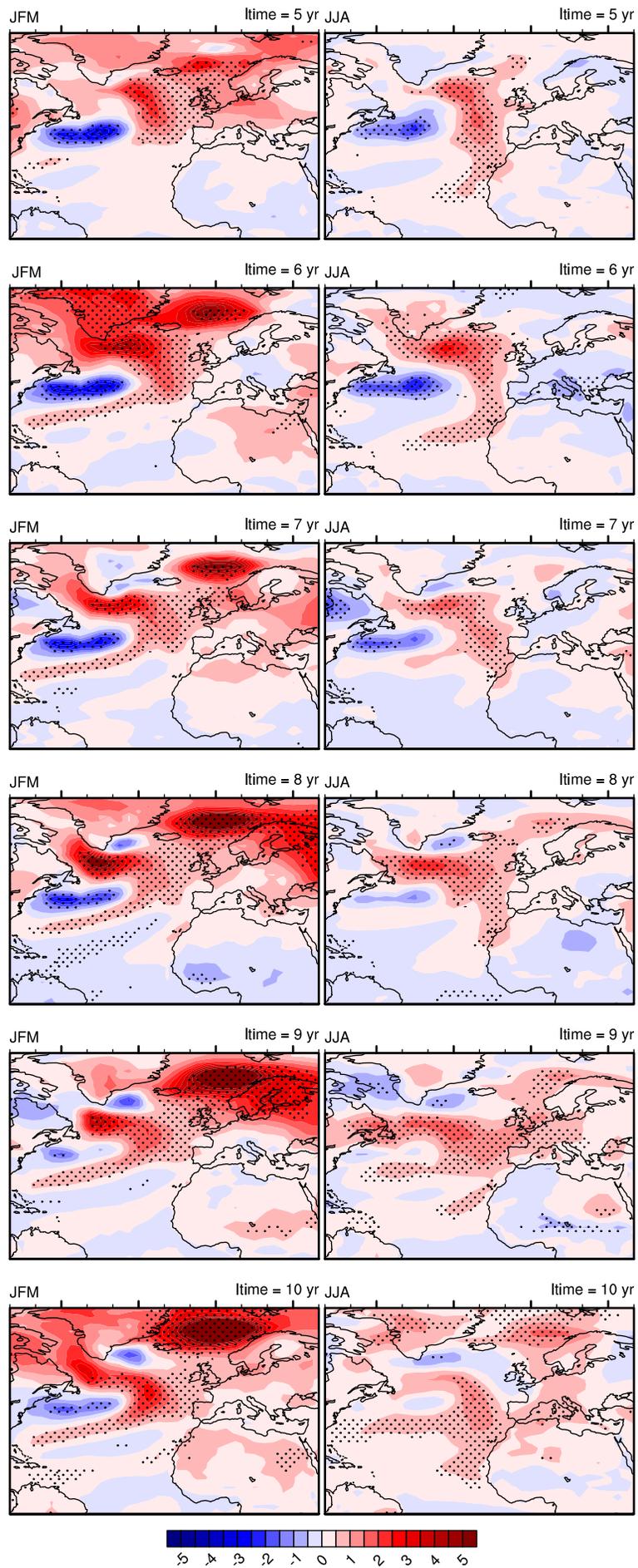
Figure 6
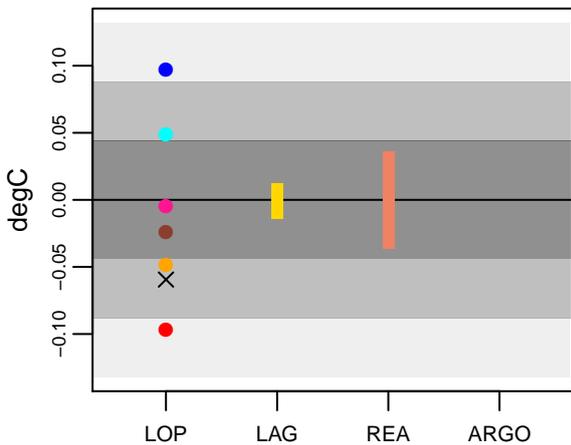
(a) NAMT (whole column)   (b) 0–300m   (c) 300–1000m   (d) 1000–2000m   (e) 2000m–bottom
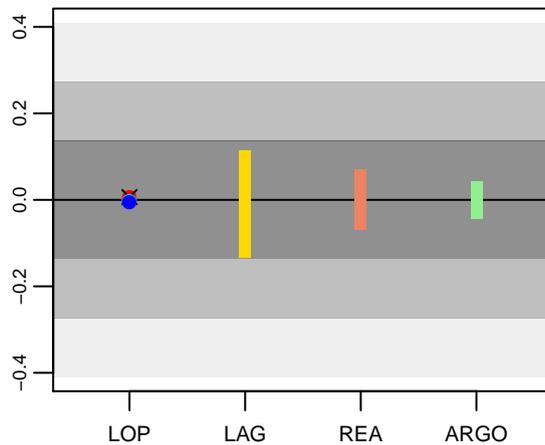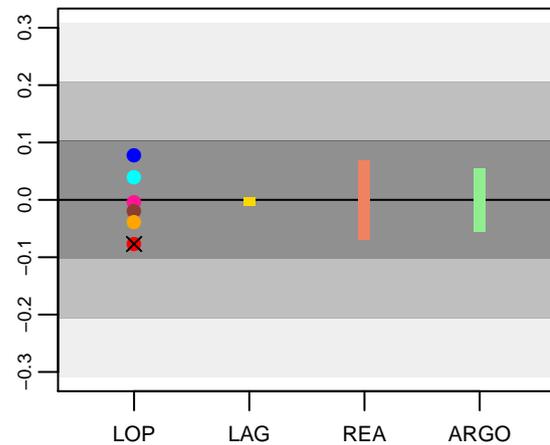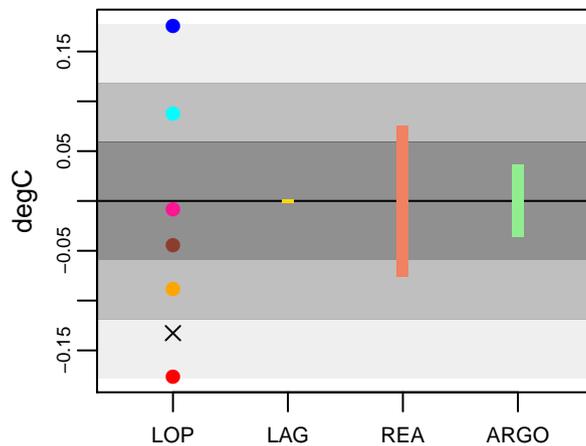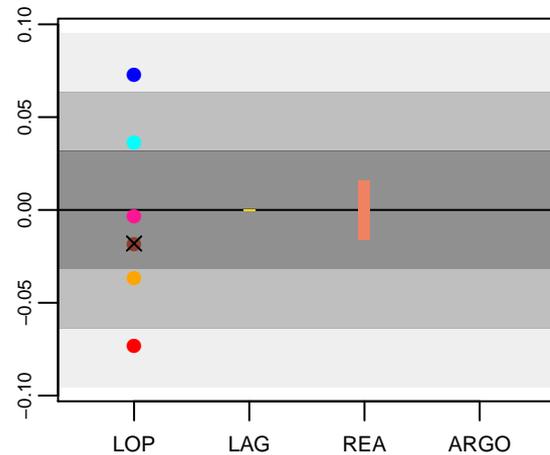
Legend:
- N20
- N10
- P01
- P05
- P10
- P20
- P20MSK
- 10-day LAG
- Reanalysis
- ARGO

Figure I